NTNU – Trondheim
Norwegian University of
Science and Technology

LED light source for hyperspectral fluorescence imaging

Nils Ove Tendenes

Master of Science in Electronics
Submission date: July 2012
Supervisor: Lise Lyngsnes Randeberg, IET

Norwegian University of Science and Technology
Department of Electronics and Telecommunications

NTNU

Norwegian University of
Science and Technology

LED light source for hyperspectral fluorescence imaging

N.O. Tendenes

July 2, 2012

nils.ove@tendenes.com

Abstract

This report deals with the possibility of creating a LED light source, to be used with hyperspectral fluorescence imaging. There are commercially available light sources that could be used, but they are expensive, they do not necessarily emit the right wavelength, the uniformity of the field is questionable and they are difficult to modify.

First a batch of Light emitting diodes were acquired, these were subjected to a series of tests to classify their limitations and determine which diodes were to be included in the final light source. A spectrometer was used to determine the emitted wavelength of each diode and which scenarios could change the wavelength of the emitted light. A photodiode was used to acquire the viewing angle of the LEDs and their relative radiant power. Images gathered by a hyperspectral camera were used to determine the relevancy of noise produced by the current source. When the light emitting diodes were chosen, the photodiode was used to make an image of the light field. The final light source was mounted on the hyperspectral camera to gather fluorescent images.

The final tests revealed a fully functional light source with potential to be used on a regular basis, but the current source was too cumbersome and the field was not optimal. These are issues that can be dealt with and this light source can in the future provide a cheap and easily modifiable light source alternative.

Preface

This master thesis has been a bit of a roller coaster to complete, with calm periods which suddenly transforms into chaos and stress. But overall it has been great fun, interesting and I have learned a lot.

I am not the only one who deserves credit for this completed document. First of all I need to thank my supervisor, associate professor Lise Lyngsnes Randeberg, for invaluable help and for basically giving me a sense of direction. A thank you as well to Martin Denstedt and Lucas Paluchowski for their enthusiasm, input and good ideas.

I also need to thank Ingulf Helland and Cu van Nguyen for their work on the constant current regulators. And Tore Landsem for taking the time to make me a few diffusers and the corresponding aluminum capsules.

Finally I would like to thank my good friends John Arne, Jarl and Håkon for both their willingness to take breaks with me and for proofreading everything I write.

Contents

1. Introduction

Hyper spectral fluorescence imaging requires a highly radiant light source with a wavelength that closely matches the excitation wavelength, to excite the fluorophore and achieve a detectable amount of emission photons. The light source would traditionally be a laser or a broad spectrum lamp, but recent advances in light emitting diode technology has made it a viable alternative. The most notable advances, in regards to hyper spectral fluorescence imaging, being higher intensity and more available wavelengths.

LED light sources have several advantages over other alternatives, the price of the final light source being one. Lasers are expensive and LEDs are quite cheap, though broad spectrum lamps often are relatively cheap, the process of suppressing undesirable wavelengths are not. Minimal heat output, fast switching and linear properties are good tools for protecting the sample from heat, overexposure of light and mechanical vibrations. Other favorable properties are small size, emission stability and long life span.

This work focuses on the prospect of designing a LED light source to be used with the hyper spectral camera VNIR-1600 from NEO. First by characterizing the chosen light emitting diodes and then studying the fluorescent output of a fluorophore excited by the light emitting diodes.

Relevant theory is presented in section 2. The methods and instruments used in the measurements is described in section 3. The results are presented in section 4, and subsequently discussed in section 5.

2. Theory

2.1. Optical properties

At the boundary between two media an incident ray of light is split into two, one part is reflected and the other is refracted. The angle of reflection equals the angle of incidence and the angle of refraction follows Snell's law:

$$n_1 \sin\theta_1 = n_2 \sin\theta_2 \tag{1}$$

Where n_1 is the refractive index of the original media, n_2 is the refractive index of the other media, θ_1 is the incident angle and θ_2 is the refracted angle.[1]

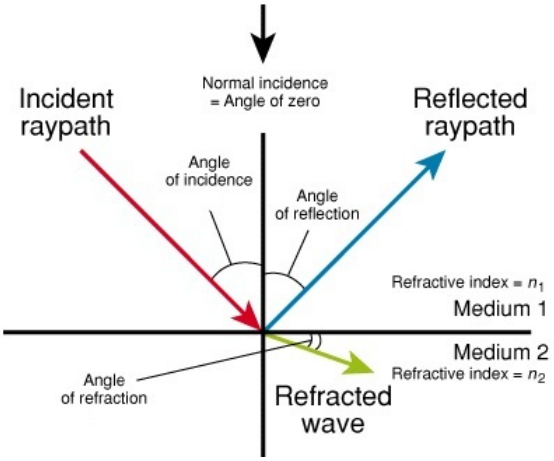

Figure 1: Ray path of refraction and reflection. Figure from glossary.oilfield.slb.com.

When the photon beam enters a biological media the interaction between photons and matter can be divided in to two different types, absorption and scattering. In absorption the frequency of the photon resonates with the natural frequency of a particle, the resonating object will be excited into a higher energy state and the photon does not survive the interaction, as it is transformed into heat motion or vibrational energy. In biological tissues, absorption is mainly caused by either water molecules or macromolecules such as proteins and pigments[6][18]. In tissue a photon will experience scattering because it interacts with a particle or structures in the medium, these scattering structures range from cell membranes to whole cells. Particles and structures which has a different refractive index, compared to the surrounding medium, and has a size that matches the wavelength will scatter the photons more strongly than other structures. When the photon experiences a change in the refractive index, the photons speed will change with a fraction that coincides with the change in refractive index. This leads to a change in the direction of the propagating photon. The scattering in tissue can be divided into two types, Rayleigh- and Mie scattering. Scattering of photons by particles of the same size order as its wavelength is described by the Mie theory, and Rayleigh scattering is scattering by particles much smaller than the wavelength[2][14][18].

In most biological tissues photons are scattered in a forward direction, a phenomenon that is not completely explained by Mie theory, and not described at all by Rayleigh scattering. Therefore the anisotropy factor is introduced:

$$g = \overline{\cos(\theta)} \tag{2}$$

The anisotropy factor gives the probable direction of scattered photons, it is defined as the average of the cosine to the scattering angle. Purely back scattered light gives a g of - 1, +1 equals purely forward scattered light and 0 is totally isotropic scattering[18].

The probability of a photon penetrating the media to a depth of x, without being absorbed or scattered, can be found from the Beer-Lambert law:

$$P(x) = P_0 e^{\mu_t x} \tag{3}$$

Where P is the radiant power, μ_t is the extinction coefficient and x is the depth[17]. The extinction coefficient is the probability of a photon interacting with the media per unit path length, and is defined by:

$$\mu_t = \mu_a + \mu_s \tag{4}$$

The absorption coefficient, μ_a, is defined as the probability of photon absorption in the media per unit path length, and the scattering coefficient, μ_s, is defined as the probability of photon scattering in the media per unit path length.

To find the reduced scattering coefficient the anisotropy factor and the scattering coefficient are combined. The scattering mean free path is defined as $l_s = 1/\mu_s$, which is the mean distance between each scattering event. The reduced mean free path gives the distance where photons have lost all information about the original incident direction and is found by combining the scattering mean free path with the anisotropy factor, $l_s^{'} = l_s/(1-g)$. The reduced scattering coefficient is then given by $\mu_s^{'} = 1/l_s^{'}$. The penetration depth of light into the media is defined as the depth where the intensity of the incident beam is reduced to $1/e$ of its original value, and is determined by;

$$\delta = \sqrt{1/(3\mu_{tr}\mu_a)} \tag{5}$$

The total transport coefficient, μ_{tr}, is found by combining the effect of absorption and the reduced scattering coefficient, it describes the total effective attenuation[8][15].

2.1.1. Luminescence

The absorption of a photon by a molecule excites an electron to a higher energy molecular orbital. The electron will then relax itself to its ground state as fast as possible. This deactivation is called luminescence when it involves emission of light. The figure 2 shows a potential energy diagram of the basic transitions in luminescence.

Luminescence can be separated into two types, fluorescence and phosphorescence. In fluorescence the excited electron has opposite spin to the second electron in the ground state orbital, which is called balanced spin (e.g. $s1 = +1/2$, $s2 = -1/2$, $S = \sum s_j = 0$) and singlet spin multiplicity ($M_s = 2S + 1 = 1$). Other types of fluorescence exists, such as fluorescence from the second excited state and doublet-doublet fluorescence, but the singlet-singlet transition between the first excited state and the ground state is, by far, the most common. In fluorescence the spin of the excited electron is opposite to that of the second electron in the ground state, this means that the relaxation process is spin allowed and therefore rapid.[1][7][13]

Phosphorescence is emission of light from triplet excited states, the excited electron has the same spin orientation as the second electron in the ground state. Which results in

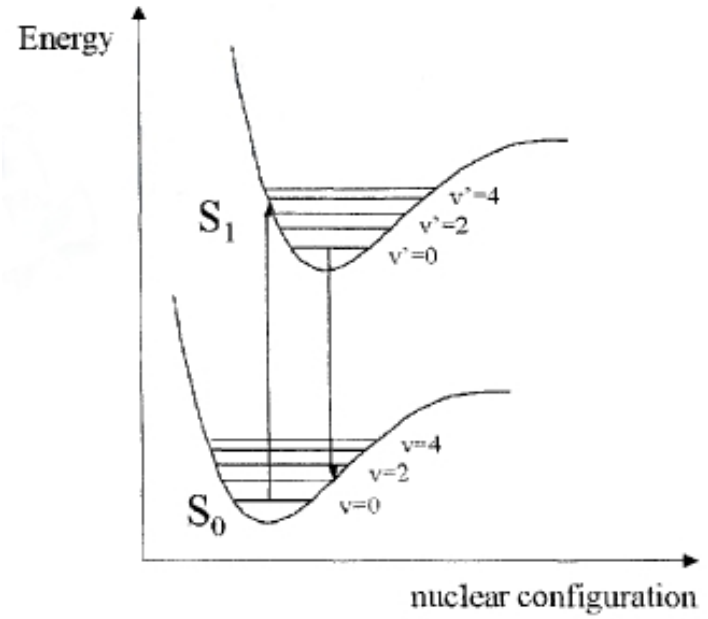

Figure 2: Potential energy diagram showing absorption and emission transitions between vibrational sub-levels in ground and electronically excited states. Figure from [13].

an overall spin of 1 (e.g. $s_1 = +1/2$, $s_2 = +1/2$, $S = \sum s_j = 1$) and a spin multiplicity of 3 ($M_s = 2S + 1 = 3$). Relaxation to the ground state is now spin forbidden and it is therefore typically a slow process.[1][7][13]

It is a rare occurrence that the emitted photon holds the same wavelength as the absorbed photon, most often there is a loss of energy. The loss of energy results in fluorescence emitted photons with longer wavelengths than the absorbed photons, this phenomenon is called the Stokes shift, see figure 3. The Stokes shift can be explained by internal conversion and internal vibrational relaxation. The excited electron is rarely excited directly to the lowest vibrational state of the S_1 state, most often it is excited to a state of higher electronic energy. Internal conversion and internal vibrational relaxation are illustrated in the figure 4. [1][7][13]

Non-radiative transition between states of different multiplicity is denoted intersystem crossing. It occurs when the spin of an excited electron is inverse and the result is that the two unpaired electrons have the same spin orientation, the overall spin, S, is 1 and the spin multiplicity, M_s, is 3, a triplet state. Intersystem crossing is formally forbidden and therefore a lot less probable than transitions between states with the same spin multiplicity. As absorption directly to a triplet state from the ground state is forbidden, intersystem crossing is an essential part of phosphorescence. Fluorescence is a spin-allowed process, phosphorescence is not. Fluorescence is therefore usually a more rapid and stronger process.[13]

The 'energy gap law' states that the rate of radiation-less transitions from one state to another is generally inversely proportional to the energy separation of the states. And since the energy separation between consecutive singlet levels tends to decrease with increasing electronic energy, non-radiative transitions between upper states occur rapidly to populate the lowest excited state, S_1. These non-radiative transitions are

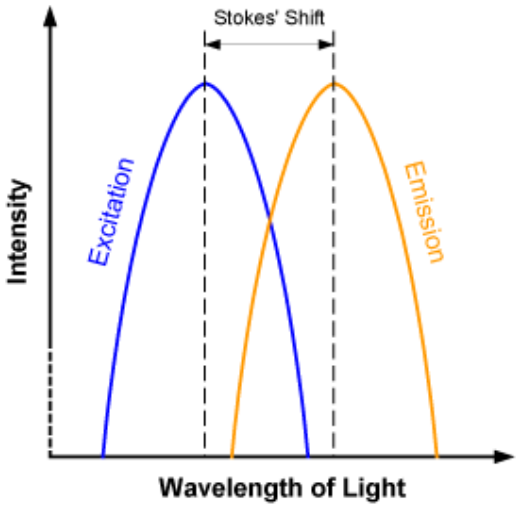

Figure 3: A representation of the Stokes shift, the wavelength of the emitted photons is usually significantly longer than the excitation photons. Figure from www.art.ca.

denoted internal conversion as they occur between states of the same spin multiplicity. The absorbance of a higher energy photon will excite the electron to a higher electronic state, but it will relax to the lowest vibrational state of S_1 before emission can occur. The emission spectrum is therefore typically independent of the excitation wavelength. [1][7][13]

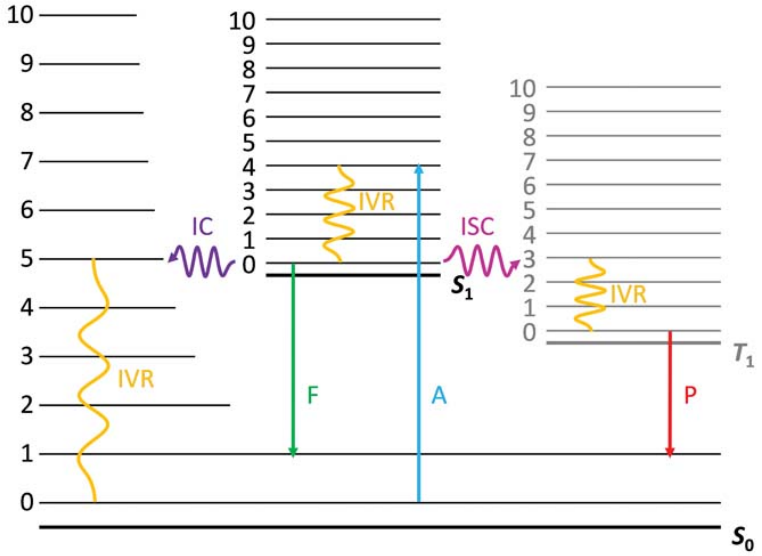

Figure 4: IVR - Internal Vibrational Relaxation, IC - Internal Conversion, ISC - Inter-System Crossing, A - Absorption, F - Fluorescence, P - Phosphorescence, 0-10 - vibrational levels of states. Figure from [9].

2.2. Hyperspectral imaging

A hyperspectral image can be considered as a collection of images of surface radiance of the same spatial area in multiple wavelength bands. It shows the total amount of photons that hits the sensor surface during the integration time, divided into different bands according to wavelength. A simple example of a spectral image is an image recorded by a digital color camera, it records an intensity image in three bands, red, green and blue. A hyperspectral image is essentially the same, but it records the intensity in up to several hundred different bands. The 2-dimensional images are recorded at discrete

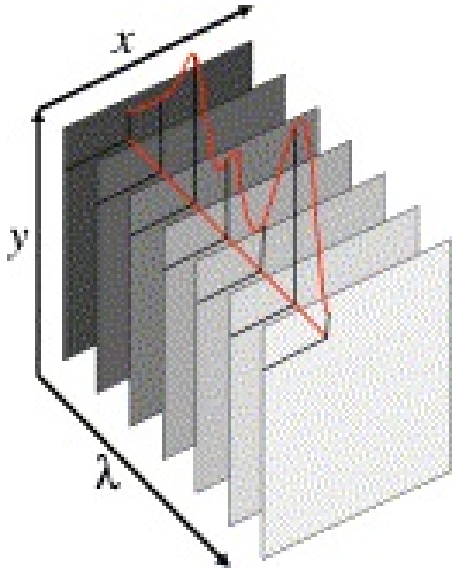

Figure 5: Two spatial axes and the third shows spectral information. Figure from sciencedirect.com.

wavelength intervals. Each image contains spatial and spectroscopic information, the information is stored as an image cube, where two axes are the spatial coordinates and the third is spectral information. Conventional spectroscopy records the intensity at every wavelength, within a spectral range, but only for a single spot. The bands of a hyperspectral image are regularly spaced over the spectrum, a continuous spectrum is measured in each pixel of the image. This technique generates large amounts of data, therefore are efficient analytical tools needed to process the data and retrieve relevant information. These tools are provided by statistically based image analysis algorithms, these can classify the pixels of the image according to statistical variance in spectral characteristics[3][11][12].

Principal Component Analysis (PCA) is a technique that transforms each pixel in the image into a point in vector space, and then chooses principal axes along the directions showing the largest variance. The data is then projected onto the chosen principal vectors. Where several principal vectors are chosen, each vector has the direction with the most variance, but is still orthogonal with the other vectors. From this a new set of bands are produced, where the first band contains most variance, the second band second most variance and so forth. The idea is that more variance equals more information and the first bands holds most of the information. The Minimum Noise Fraction (MNF) transform, also known as noise whitened PCA, is essentially a two step PCA process,

where the first transformation decorrelates and rescales the noise in the data, such that each image band has noise with unit variance and no band to band correlation. The first layers of the transformed image will contain coherent images with large eigenvalues. The second transformation is a standard PCA of the noise whitened data. Noise can then effectively be filtered out by removing the incoherent layers prior to inverse transformation[4][5][10].

2.3. Light emitting diodes

Electroluminescence is a phenomenon in which light is emitted by a material that is subjected to an electrical field. Injection electroluminescence is the underlying concept for any light-emitting diode. Under normal conditions the concentration of thermally excited electrons is very small, and the device will not glow. To increase the emission rate of photons an increase of excited electrons have to be created by external means. This can be achieved in many different ways, but a normal method is to forward bias a p-n junction diode. Carrier pairs are injected into the junction region and the increased number of recombinations causes the device to glow. A simple LED p-n junction is illustrated in figure 6. [1][16]

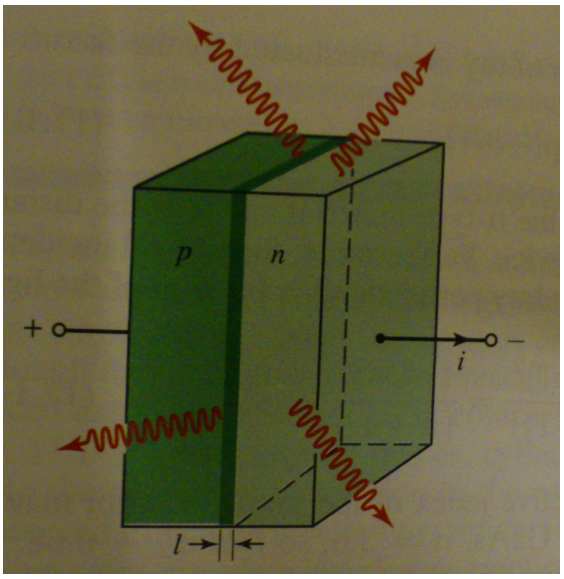

Figure 6: A forward-biased LED. Figure from [1]

In these semiconductor devices there are two important processes: the excitation of electrons into higher energy states and the relaxation of exited electrons back to empty lower states(holes). Radiative recombination is a diffusion driven process, and therefore only occurs at or near the p-n junction. In non-radiative transitions the excess energy is released in the form of phonons. [1][16]

When an electron relaxes from the conduction band to the valence band it releases excess energy in the form of a photon, similar to the boost of energy an electron needs to jump from the valence band to the conduction band. The energy of the photon, which in turn corresponds with the color of the light, is determined by the band gap of the p-n junction. The valence band, conduction band and the bandgap are illustrated by the figures 7 and 8. [1][16]

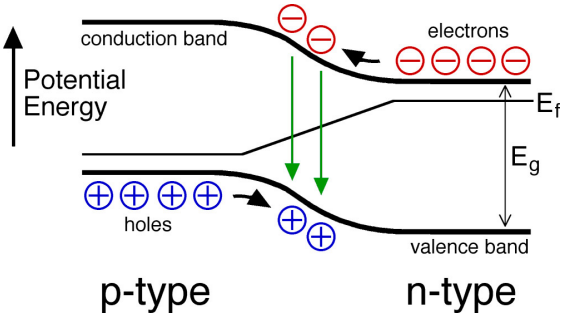

Figure 7: The band structure of a forward-biased LED. Figure from http://mrsec.wisc.edu

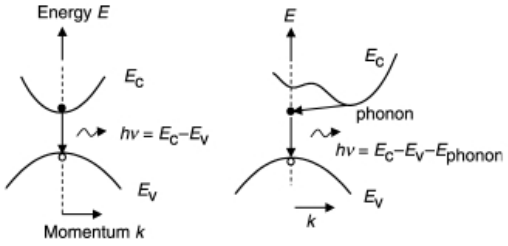

Figure 8: LEDs are usually direct bandgap, since the indirect band transition is much less probable. In materials with indirect band structure the transition needs the assistance of a phonon to conserve momentum. Left: Direct bandgap. Right: Indirect bandgap. Figure from [16]

The current voltage characteristic, 9, of an ideal light emitting diode is described by the Shockley equation:

$$I(V) = I_s(\exp((qV)/(kT)) - 1) \tag{6}$$

Where I_s is the current obtained with a reverse bias. I_s is called the saturation current and is controlled by the number of minority carriers which diffuse to the pn-junction. In this case, the current density, I_s/A, can be calculated according to:

$$I_s/A = (qD_p p_{n0})/(D_p\tau_p)^{1/2} + (qD_n n_{p0})/(D_p\tau_p)^{1/2} \tag{7}$$

where A is the cross-sectional area of the diode junction, D_n and D_p are the electron and hole diffusion constants, n_{p0} and p_{n0} are the equilibrium electron and hole concentration on the p- and n-side. Under forward bias for $V > 3kt/q$ the current rises exponentially with V. [16]

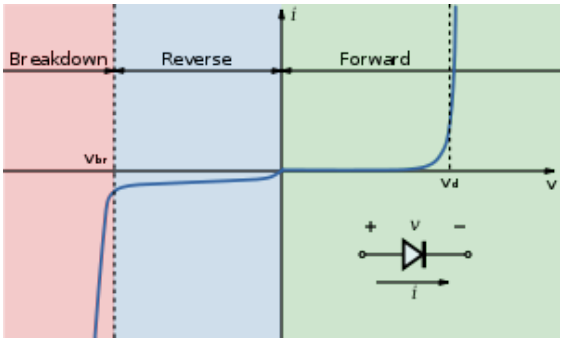

Figure 9: The I-V characteristics of a light emitting diode. Figure from mbed.org

3. Method

One hundred light emitting diodes were bought from Farnell, 10, the technical data sheet can be found in appendix A. A series of tests were performed on the diodes, to find a few diodes that performed as similar as possible. The few who were found to be similar enough were used in the final light source tests. The diodes were arranged in a matrix, for the purpose of easily identifying single diodes, 10.

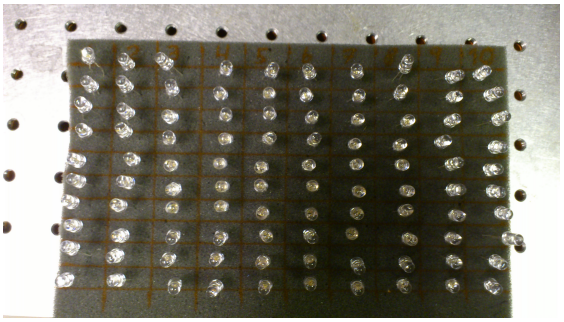

Figure 10: The diodes.

Current regulators were built for the purpose of controlling the emission of light from the diodes on an individual basis. These were built at the Department of Electronics and Telecommunications at NTNU. First a prototype with a single channel was built, which was the current source in most of the LED tests. Tests were performed on the prototype before ten more were built, 11. Information on the prototypes can be found in appendix B.

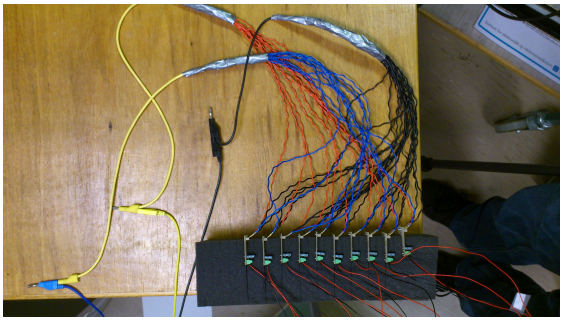

Figure 11: The final ten constant current regulators.

All hyperspectral measurements were performed using VNIR-1600, a hyperspectral camera system developed by Norsk Elektro Optikk AS (HySpex, NEO, Lørenskog, Norway). The camera is a high performance push-broom imaging spectrometer, specifications in table 1.

Module	VNIR-1600
Detector	Si CCD $1600 * 1200$
Spectral range	$0,41,0\mu m$
Spatial pixels	1600
FOV across track	$17°$
Pixel FOV across/along track	0,185 mrad/0,37 mrad
Spectral sampling	3,7 nm
# of spectral bands	160
Digitization	12 bit
Frame rate to HD	120 fps

Table 1: Specifications of the hyperspectral camera. Specifications gathered from neo.no.

3.1. LED spectrum

The first measurement performed on the diodes was a test to determine their exact wavelength spectrum. A relatively high current was sent through the diode, 16 mA, which was placed in an integrating sphere. A fiber connected to a spectrometer was also present in the sphere, the data from the spectrometer was analyzed with the software SpectraSuite. The spectra of all the diodes were collected in this way. To keep the spectrometer from saturating a damping element was introduced between the sphere and the spectrometer.

Instrument	Producer	Model
Power supply	Mascot	719
Current regulator prototype	NTNU	0
Dual channel thermometer	Tektronix	DTM920
Optical fiber	Top Sensor Systems	FC-UV600-2-15mA
Optical fiber	Ocean Optics	P200-2-UV/VIS
Damping element	Ocean Optics	
Spectrometer	Ocean Optics	SD2000
Hairdryer	BaByliss	2000
Spectrasuite (software)	Ocean Optics	5.1, Windows XP

Table 2: Instruments used in measurements of the spectrum.

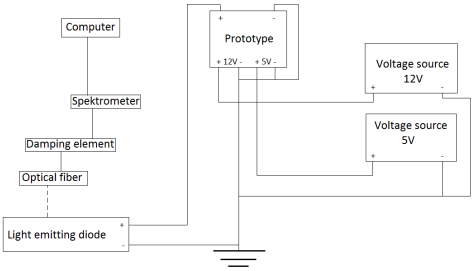

Figure 12: Schematics of the setup used during the spectrum measurements.

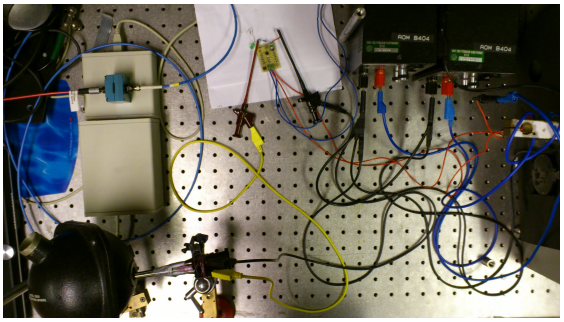

Figure 13: Picture of the setup used during the spectrum measurements.

3.1.1. Heat

Initially the equipment setup for measuring the dependence of the wavelength spectrum on heat were the same as measuring the spectrum itself. But there were two exceptions, a thermometer was present in the integrating sphere, 14, and the temperature was increased by blowing warm air from a hairdryer into the sphere.

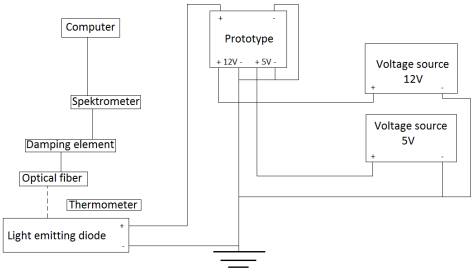

Figure 14: Schematics of the setup used during the measurements of spectrum changes due to changes in temperature.

3.1.2. Time

A few of the LEDs were also tested for changes in the spectrum over time, the setup was the same as for determining the spectrum (ref bilder). There was a constant current flow of 16 mA through the diodes and a new measurement was performed every ten minutes.

3.2. LED viewing angle

By connecting a photodetector with a lock-in amplifier and measuring the light intensity from the diode at different angles, 16, an image of the LED viewing angle could be created. Two measurements of the same diode were made, one where the feet of the diodes were horizontal with each other and one where they were vertical, the diodes were turned 90 degrees, 17. A lock-in amplifier was used to measure the signal, therefor a signal generator was used to power the LED. The signal generated was a rectangle pulse with an amplitude of two volts and an offset of two volts, a rectangle pulse that changes between four volts and ground. A resistance of 200 ohms was used to transform the signal to a rectangle pulse with an amplitude of 10 mA and an offset of 10 mA. A slit was made to reduce the angle of incidence from the LED, this slit can be seen in the figure 17. After the measurements the vertical and horizontal profiles were combined to create a three-dimensional profile. Each point in the horizontal profile was made into a vector with the same profile as the vertical profile.

Instrument	Producer	Model
Power supply	Mascot	719
PIN photodiode	UDT Sensors	10DP Lot: 9334-1
Amplifier	NTNU	B.nr.40
Lock-In Amplifier	Stanford Research Systems	SR830 DSP

Table 3: Instruments used in measurements of the viewing angle.

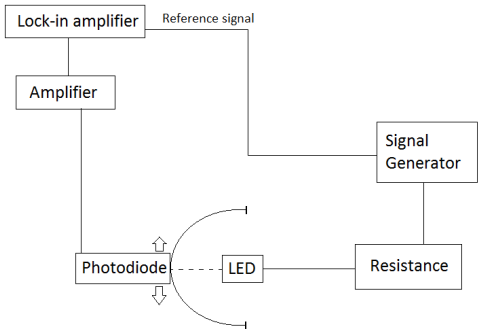

Figure 15: Schematics of the set up used during the measurements of the viewing angle.

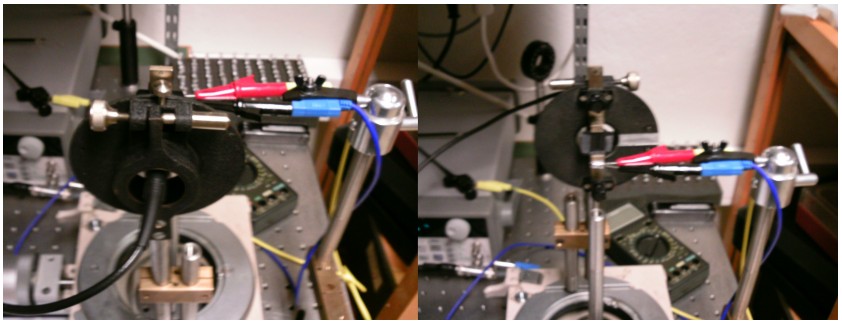

Figure 16: How the photodiode was moved into a position of plus 90 degrees, left, and minus 90 degrees, right, compared to the front of the LED.

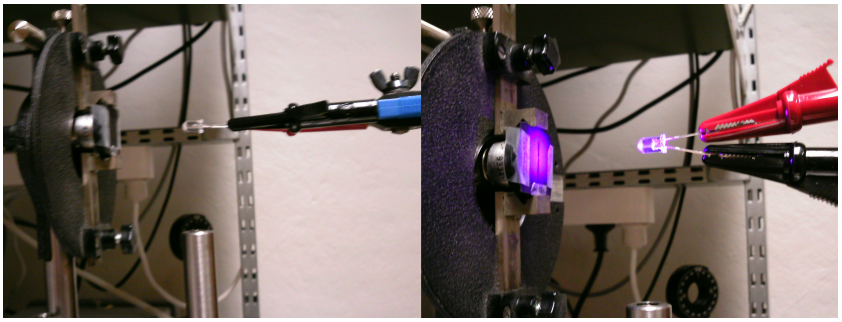

Figure 17: A LED in its horizontal, left, and its vertical position, right.

3.3. LED radiant power

A reliable method of calibrating the equipment was never available, all measurements of radiant power in this work were only used for comparing the diodes to each other. First a measurement of the diodes at 16 mA was performed and then the same measurement was performed a day later, to determine the accuracy of the method and the similarity of the diodes. The experimental set up can be seen in the figures 18 and 19, this is the set up used for all measurements of radiant power.

Instrument	Producer	Model
Power supply	Mascot	719
Digital multimeter	Meterman	37XR
Current regulator prototype	NTNU	1
PIN photodiode	UDT Sensors	10DP Lot: 9334-1
Amplifier	NTNU	B.nr.40
Digital multimeter	Solartron Schlumberger	7150 plus

Table 4: Instruments used in measurements of the radiant power.

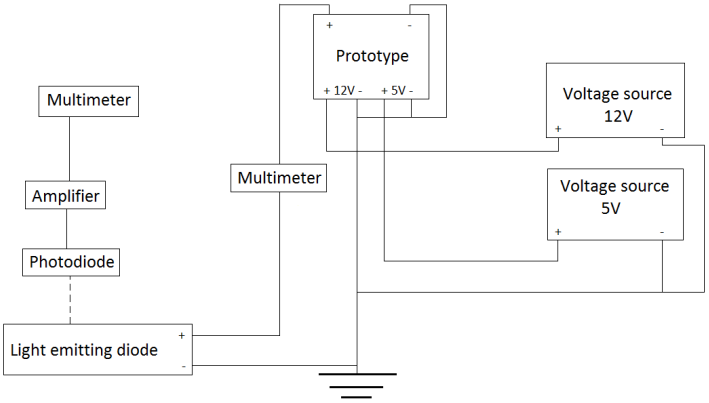

Figure 18: Schematics of the set up used during the measurements of the radiant power.

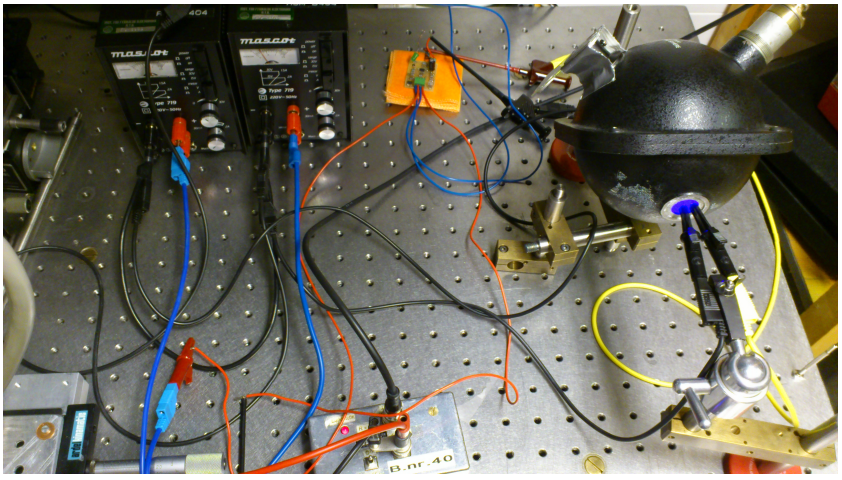

Figure 19: A picture of the set up used during the measurements of the radiant power.

3.3.1. Radiant power over time

A few of the diodes were subjected to a current of 16 mA over a period of time and a measurement of their radiant power was performed every few minutes, to determine the time-dependent changes in their radiant power.

3.3.2. Linearity of radiant power

At first the diodes were subjected to a constant high current, ≈20 mA, for a few minutes, to minimize the effect of the changes the diodes were prone to over time. Then measurements were performed with a gap of one mA, or two, between them.

3.4. Noise

There was noise from the current regulator, this noise was most probably detectable in the emitted light from the LEDs. Measurements were performed to establish the significance of this noise in hyperspectral fluorescence images.

A fluorophore was required, to characterize the LEDs' ability to excite the fluorophore and determine how much noise was transmitted throughout the process. The

Instrument	Producer	Model
Power supply	Mascot	719
Digital multimeter	Meterman	37XR
Current regulator prototype	NTNU	1
Hyperspectral camera	NEO	VNIR 1600
LED flashlight	LED LENSER	Hokus Focus 694256
Spectral reflectance reference	Top Sensor Systems	WS-2
Linear filter	Carl Zeiss	4338500
ENVI (software)	Exelis	4.4, Windows XP

Table 5: Instruments used in measurements with the hyperspectral camera.

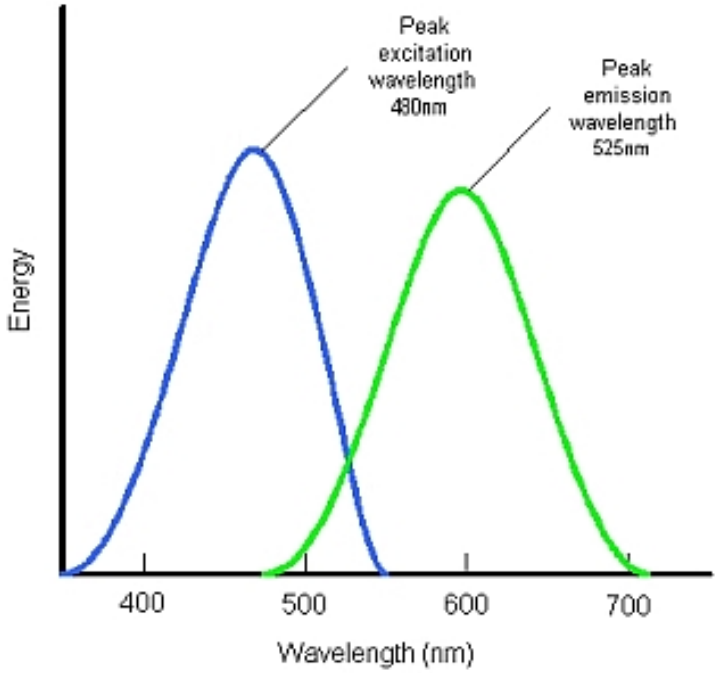

Figure 20: The excitation and emission wavelength of Fluorescein sodium, image from opsweb.org.

fluorophore chosen was Fluorescein sodium with the concentration $0.7272g/l$, both for its availability and excitation wavelength, which can be seen in figure 20. A schemtaic of the set up is shown in the figure 21, the LED excites the fluorophore and the emission wavelength is detected by the camera. First the emitted light was measured over a period of time, the camera was held in the same position over the same line of pixels. The y-axis in the hyperspectral image shows how the intensity of this line of pixels change over time. Two measurements were performed on three diodes, one with a frame period of 10 ms and one with a 20 ms frame period, in all the measurements the integration time was 8 ms and the binning value was 2x. After the images were captured they were analyzed with the software ENVI. A value of the x-axis with a high intensity value was chosen, and a range of four hundred lines were selected from this x-value. This range is depicted in four different wavelengths. One wavelength where the intensity is influenced by the light from the LED and fluorescence from the paper.

Two where the intensity was close to zero, one lower and one higher than the emission wavelength. And one of the wavelengths was as close to the peak of the emitted light as possible.

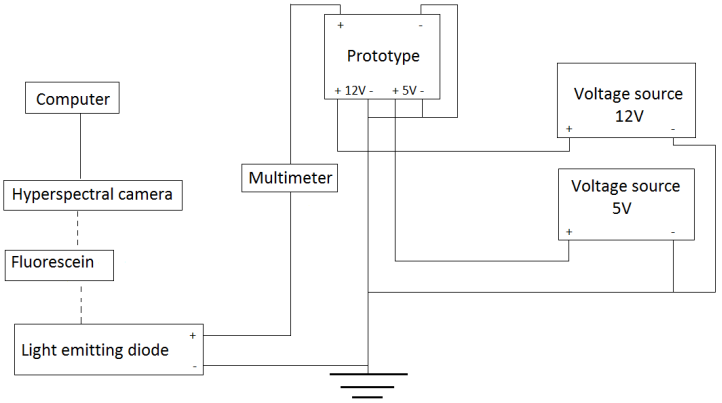

Figure 21: The schematics of the set up used when determining the significance of the noise in the light source.

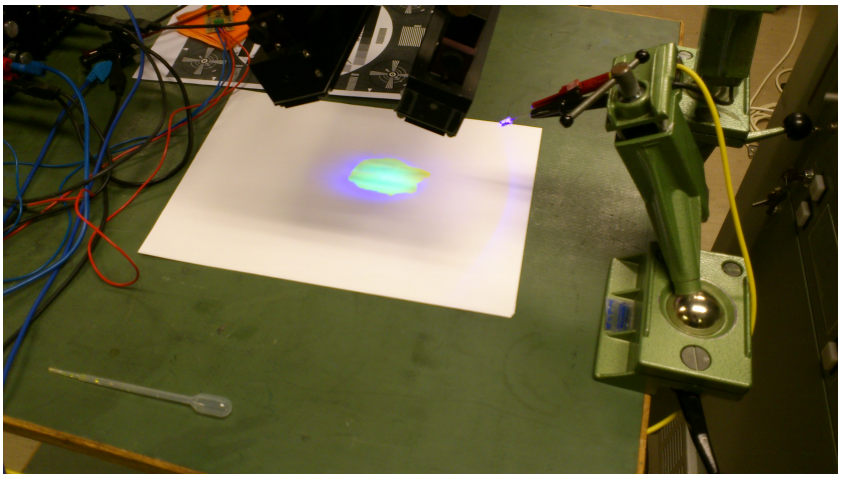

Figure 22: Fluorescence due to excitement by a light emitting diode.

A LED flashlight was used as a reference light source, it was known to be quite noise free. As the flashlight emitted white light a linear filter was used to filter out all but the emission wavelength of fluorescein. The set up can be seen in 23.

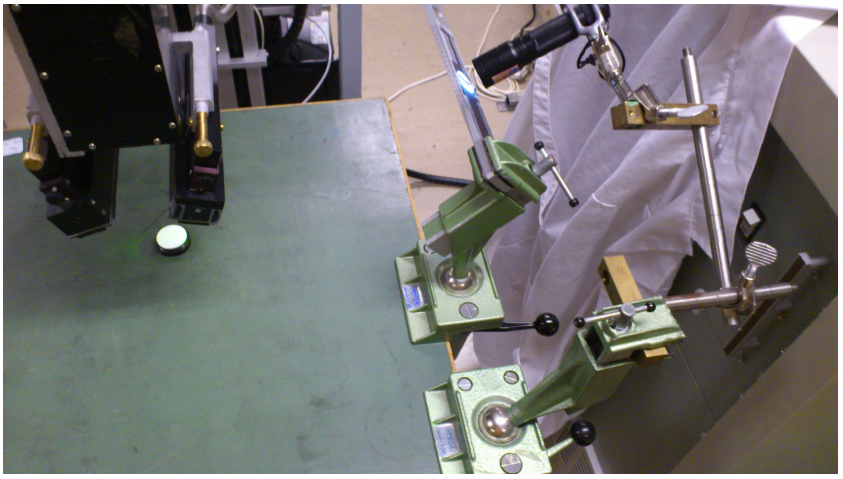

Figure 23: The mounted reference light source illuminates a spectral reflectance reference.

3.5. LED light source

Light emitting diodes were attached to an aluminum capsule, this capsule had the possibility to attach a diffuser opposite to the LEDs. And a cylindrical lens could be fastened to the capsule. Three aluminum capsules were built at Department of Electronics and Telecommunications at NTNU, all with a corresponding diffuser. Four different tests of the field produced by the light source were performed. First a measurement of the field produced with only the diodes, second a measurement of the field with the lens, third a measurement with the diffuser and then the field was measured with both the diffuser and the lens attached. The photodiode was attached to the hyperspectral camera, so that the cameras translation stage could be used in the field measurements.

A group of ten diodes were found by comparing the wavelength spectrum of the diodes against their radiant power, they were very similar and were therefore chosen to be used in the final light source. These diodes were 2-3, 2-9, 3-5, 3-9, 4-6, 4-8, 5-7, 6-8, 7-8 and 7-10.

First the four different field measurements were performed with a single diode active in the light source. The current regulator was set to 16 mA. Afterwards there were always ten active diodes in the light source, but the distance between diodes was changed. There were three aluminum capsules made, one with a distance of 0,75 cm between the center of each diode, another with 1,00 cm between the diode centers and a third with the distance 1,25 cm from one center to the next. The figures 24, 25 and 26 show how the light within the viewing angle of each diode will affect the others. The four different field measurements were performed with ten active diodes in each of these three capsules. The diodes were initially subjected to a current of 18 mA in these measurements, but the field was prone to a lot of neighbour effects when the distance between the diode centers were 0,75 cm. The current subjected to the diodes was changed individually to achieve a uniform field.

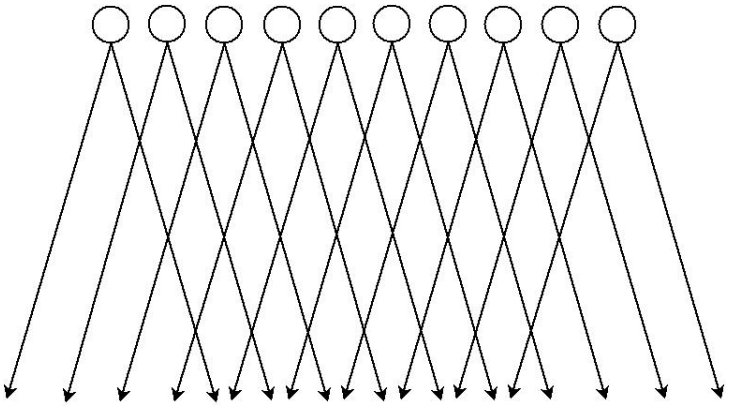

Figure 24: The light lines of the ten light emitting diodes viewing angle in the source where they are divided by 0,75 cm.

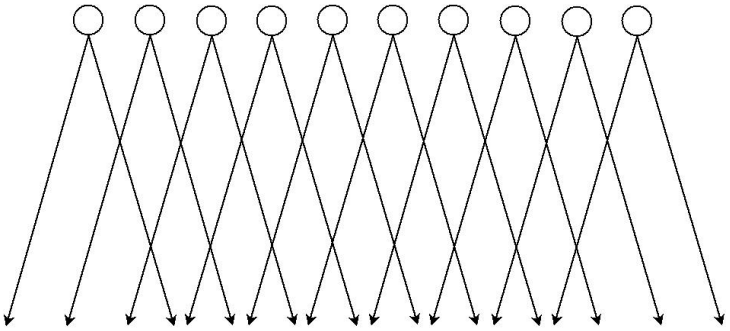

Figure 25: The light lines of the ten light emitting diodes viewing angle in the source where they are divided by 1,00 cm.

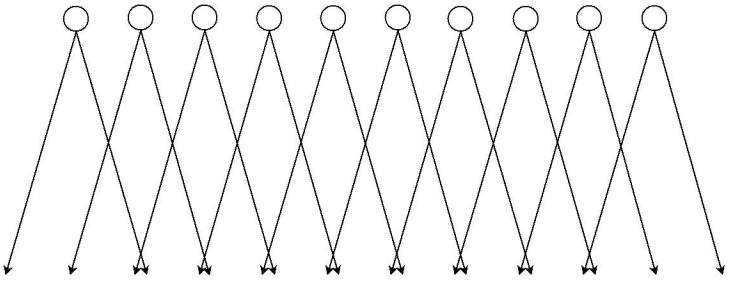

Figure 26: The light lines of the ten light emitting diodes viewing angle in the source where they are divided by 1,25 cm.

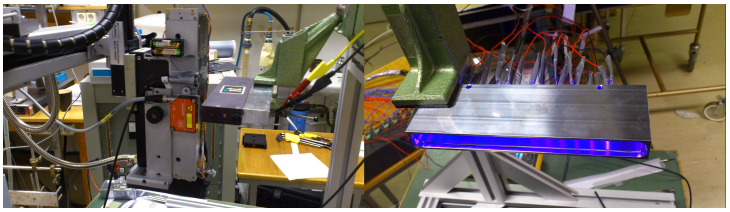

Figure 27: The left side shows the aluminum capsule with the lens attached and perpendicular to it is the photodiode attached to the camera. The right side shows the final light source, without the diffuser or lens.

When the field measurements were performed the light source was positioned as can be seen in the image 27, the photodiode was placed in the center of the generated field and $\approx$ 10 cm from the capsule, as this was not an abnormal distance from the light source to the object in hyperspectral imaging. Measurements were performed in intervals of 1 cm up to 8 cm from the center in both directions of the horizontal plane. This line of measurements were also performed 1,5 cm over and under the center in the vertical plane.

The capsule with 1,25 cm between the center of each diode was mounted as a light source for the hyperspectral camera, and a few different images of fluorescein were acquired. First fluorescein was put on paper, both as drops and in a larger puddle. Thereafter fluorescein was put in containers, to achieve a more homogeneous surface. The containers were a cylindrical test tube and a weighing ship. The images were subjected to noise reduction, by the MNF transform present in the software ENVI, version 4.4. The spectrum was acquired from different points in the image, points which in theory should have the same spectral response, and these points were compared to each other.

4. Results

4.1. LED spectrum

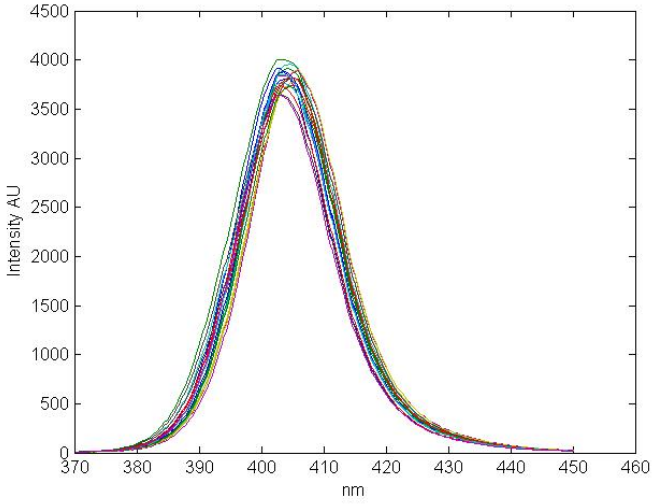

Figure 28: The measured spectra of the diodes.

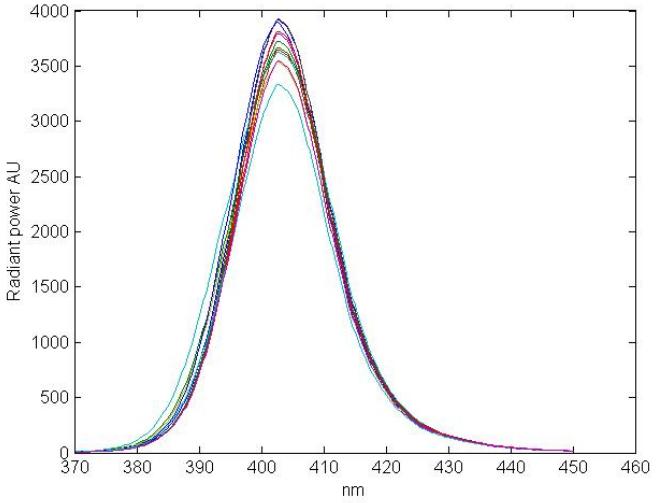

Figure 29: Spectra of the diodes with the peak at 402,68 nm. The diodes represented are 1-2, 1-8, 2-10, 5-1, 5-6, 6-4, 7-5, 8-4, 8-6, 9-9, 10-8 and 10-9.

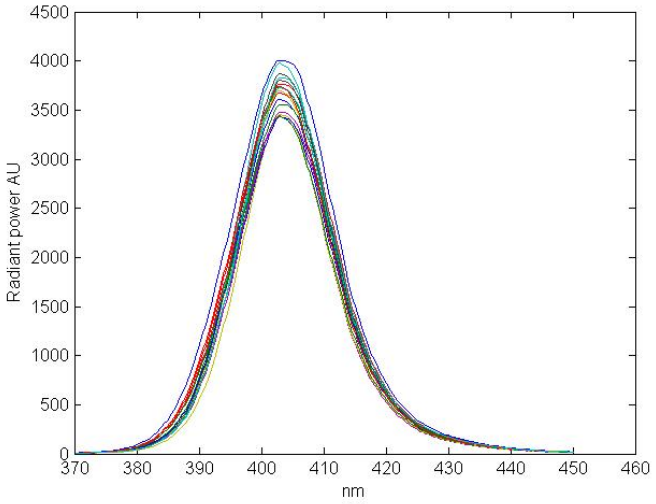

Figure 30: Spectra of the diodes with the peak at 403,05 nm. The diodes represented are 1-3, 2-1, 2-2, 4-4, 5-9, 5-10, 6-6, 7-3, 7-6, 8-1, 8-2, 8-3, 8-8, 8-9, 9-1, 9-5, 10-3 and 10-6.

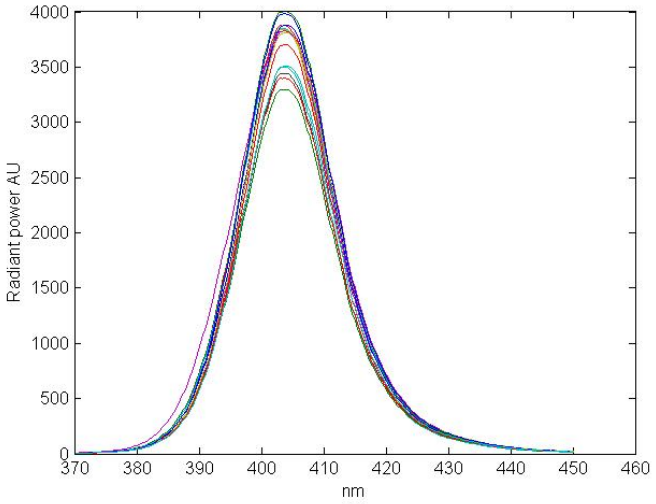

Figure 31: Spectra of the diodes with the peak at 403,77 nm. The diodes represented are 1-9, 2-3, 2-6, 2-9, 3-5, 3-9, 4-6, 4-8, 5-3, 5-7, 6-3, 6-7, 6-8, 7-8, 7-10, 9-2 and 10-5.

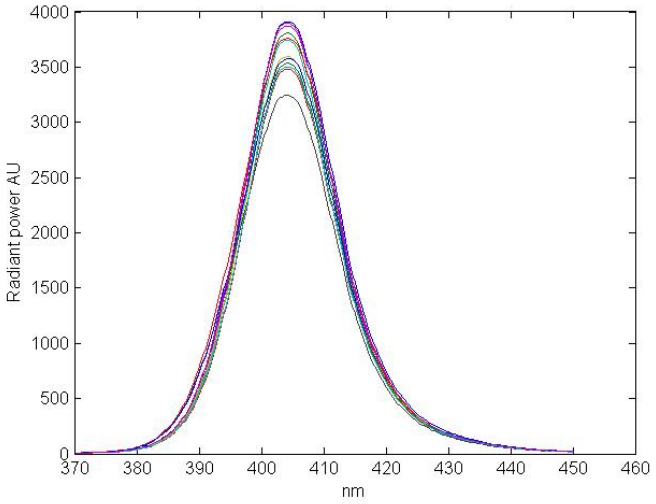

Figure 32: Spectra of the diodes with the peak at 404,14 nm. The diodes represented are 1-10, 3-4, 4-9, 4-10, 5-4, 6-10, 7-7, 9-3, 9-4, 9-8, 10-2 and 10-4.

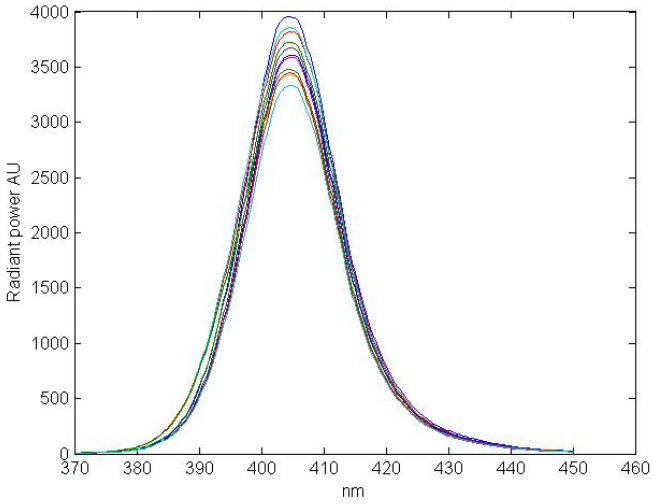

Figure 33: Spectra of the diodes with the peak at 404,50 nm. The diodes represented are 1-5, 2-7, 2-8, 4-5, 5-5, 6-5, 8-7, 9-6, 10-1, 10-7 and 10-10.

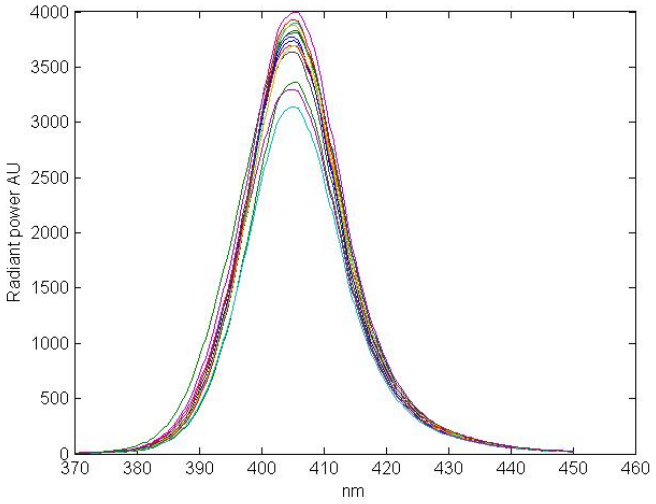

Figure 34: Spectra of the diodes with the peak at 405,22 nm. The diodes represented are 1-4, 2-5, 3-2, 3-8, 4-2, 4-3, 4-7, 5-8, 6-1, 6-2, 7-1, 7-2, 7-9 and 9-7.

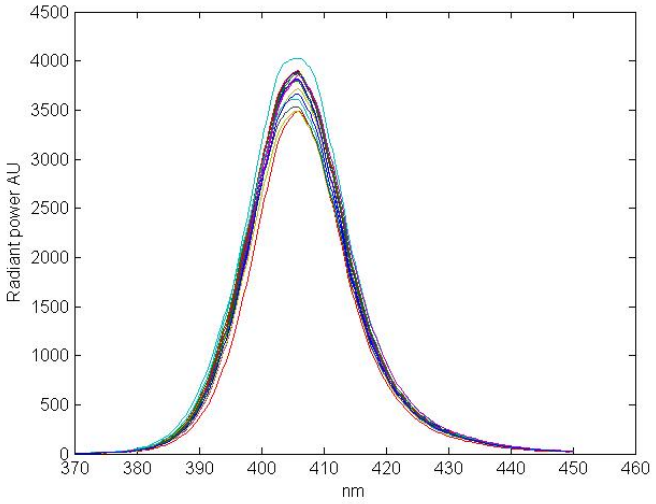

Figure 35: Spectra of the diodes with the peak at 405,95 nm. The diodes represented are 1-6, 1-7, 2-4, 3-1, 3-3, 3-6, 3-7, 3-10, 4-1, 5-2, 6-9, 7-4, 8-5, 8-10 and 9-10.

4.1.1. Heat

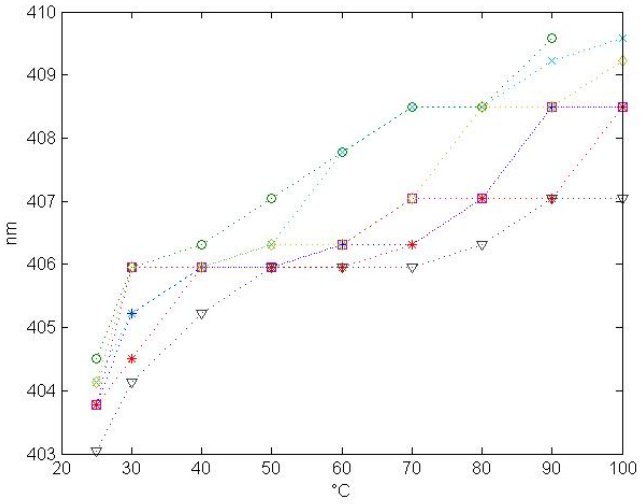

Figure 36: How the value of the peak of the emitted wavelength changes due to temperature change. The diodes and their corresponding symbol: 1-9 plus, 2-7 circle, 2-9 star, 6-10 x, 7-8 square, 9-4 diamond, 10-3 delta.

4.1.2. Time

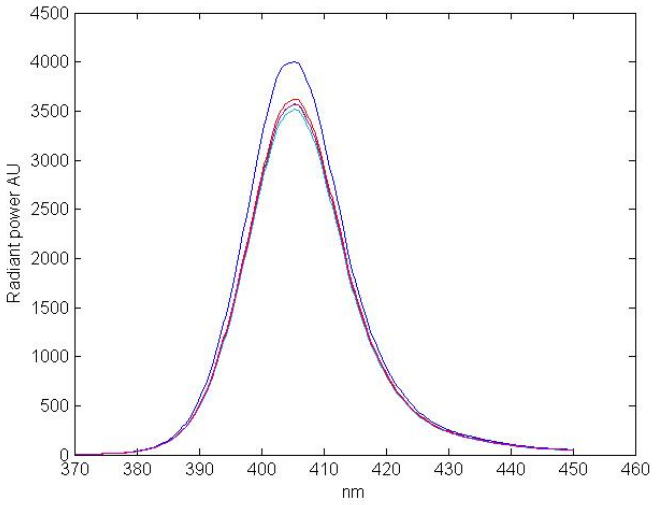

Figure 37: Several measurements of the spectrum of diode 4-9, each measurement 10 minutes apart.

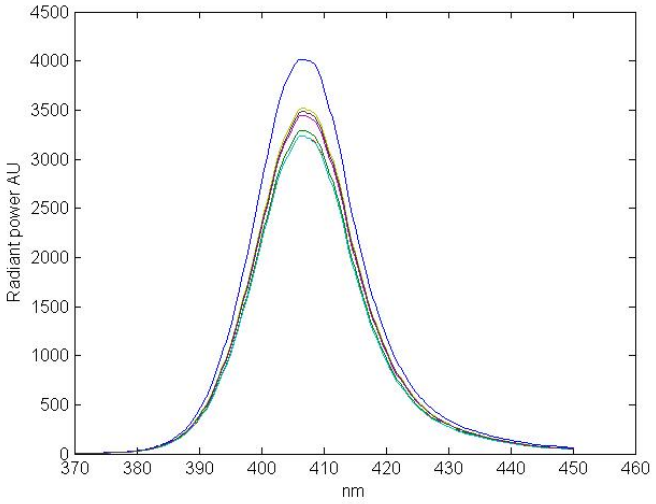

Figure 38: Several measurements of the spectrum of diode 7-4, each measurement 10 minutes apart.

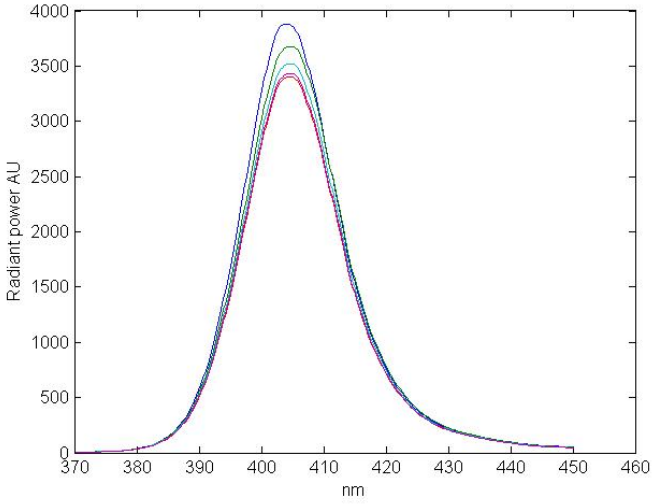

Figure 39: Several measurements of the spectrum of diode 8-2, each measurement 10 minutes apart.

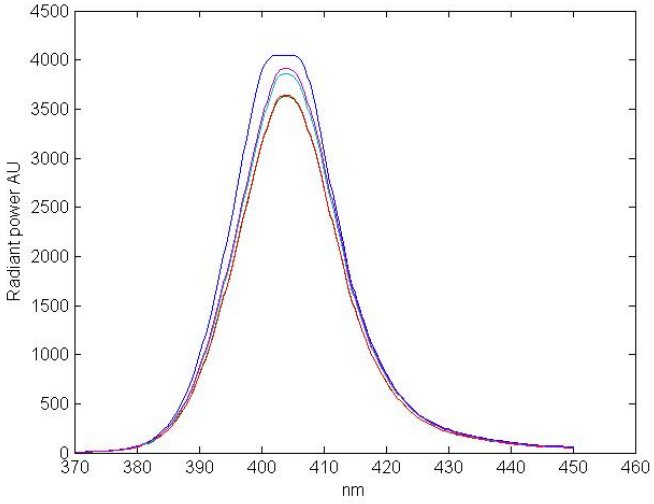

Figure 40: Several measurements of the spectrum of diode 10-8, each measurement 10 minutes apart.

4.2. LED viewing angle

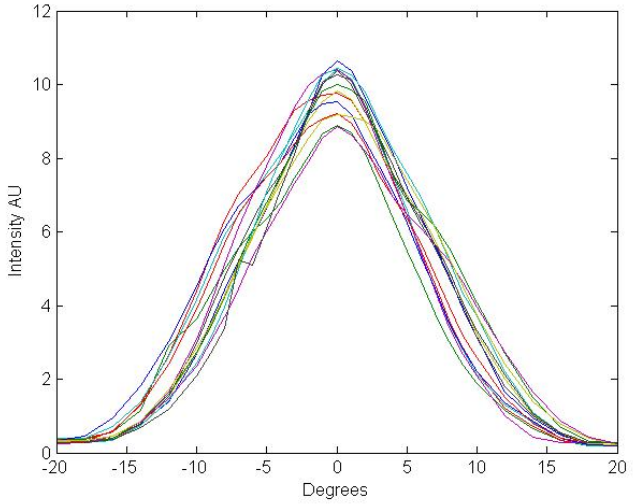

Figure 41: The measured viewing angle of 14 diodes at the horizontal position.

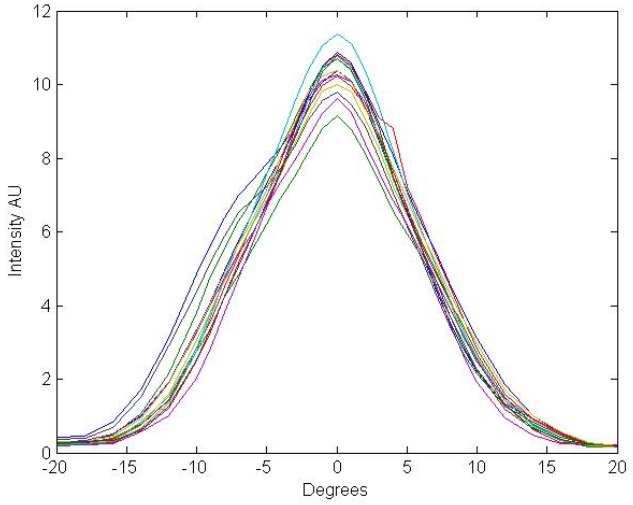

Figure 42: The measured viewing angle of 14 diodes at the vertical position.

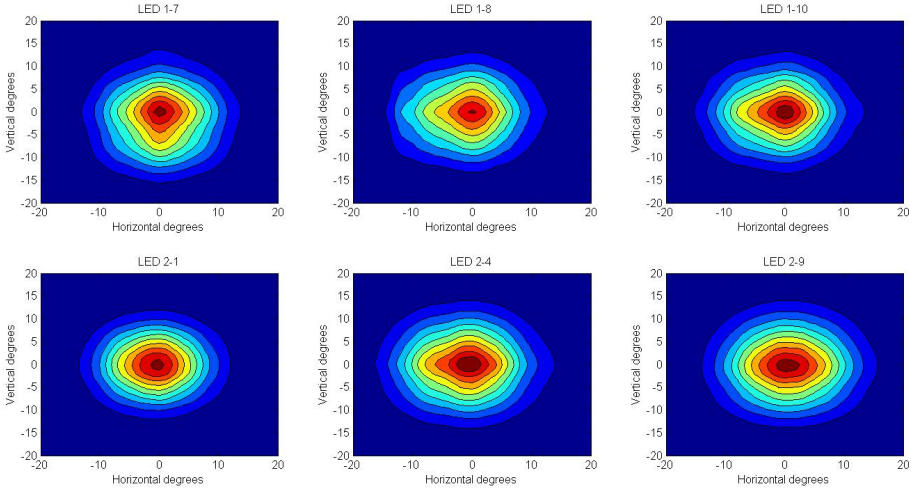

Figure 43: Intensity profile of six diodes.

4.3. LED radiant power

LED	AU	AU	%	LED	AU	AU	%
1-1	-	-	NA	4-1	1,18	1,18	0,0%
1-2	-	0,99	NA	4-2	1,08	1,10	1,9%
1-3	-	1,02	NA	4-3	1,14	1,14	0,0%
1-4	-	1,13	NA	4-4	1,09	1,09	0,0%
1-5	-	0,99	NA	4-5	1,08	1,08	0,0%
1-6	-	1,15	NA	4-6	1,13	1,13	0,0%
1-7	-	0,96	NA	4-7	1,17	1,16	0,9%
1-8	-	1,05	NA	4-8	1,12	1,12	0,0%
1-9	-	1,05	NA	4-9	1,13	1,13	0,0%
1-10	-	1,09	NA	4-10	0,97	0,95	2,1%
2-1	1,02	0,95	7,4%	5-1	0,86	0,85	1,2%
2-2	1,02	1,03	1,0%	5-2	1,04	1,03	1,0%
2-3	1,09	1,10	0,9%	5-3	1,05	1,04	1,0%
2-4	1,14	1,13	0,9%	5-4	1,10	1,09	0,9%
2-5	1,14	1,14	0,0%	5-5	1,10	1,10	0,0%
2-6	0,99	0,98	1,0%	5-6	1,04	1,03	1,0%
2-7	1,03	1,02	1,0%	5-7	1,07	1,06	0,9%
2-8	1,06	1,05	1,0%	5-8	1,20	1,19	0,8%
2-9	1,07	1,08	0,9%	5-9	1,00	0,99	1,0%
2-10	1,08	1,08	0,0%	5-10	1,12	1,10	1,8%
3-1	1,04	1,03	1,0%	6-1	1,19	1,17	1,7%
3-2	1,15	1,06	8,5%	6-2	1,16	1,13	2,6%
3-3	1,15	1,16	0,9%	6-3	0,91	0,90	1,1%
3-4	1,07	1,08	0,9%	6-4	0,99	0,98	1,0%
3-5	1,12	1,12	0,0%	6-5	1,04	1,03	1,0%
3-6	1,14	1,14	0,0%	6-6	1,16	1,16	0,0%
3-7	1,16	1,16	0,0%	6-7	1,17	1,16	0,9%
3-8	1,13	1,13	0,0%	6-8	1,13	1,13	0,0%
3-9	1,13	1,12	0,9%	6-9	1,12	1,12	0,0%
3-10	1,12	1,12	0,0%	6-10	0,97	0,98	1,0%

Table 6: Two measurements of the intensity of the different light emitting diodes at 16 mA, and the percentage of difference between them.

LED	AU	AU	%	LED	AU	AU	%
7-1	1,07	1,08	0,9%	9-1	0,91	0,91	0,0%
7-2	1,08	1,08	0,0%	9-2	1,17	1,18	0,9%
7-3	1,07	1,06	0,9%	9-3	1,08	1,09	0,9%
7-4	0,97	0,98	1,0%	9-4	1,11	1,12	0,9%
7-5	1,09	1,10	0,9%	9-5	1,07	1,08	0,9%
7-6	1,13	1,12	0,9%	9-6	1,04	1,05	1,0%
7-7	1,10	1,10	0,0%	9-7	1,17	1,17	0,0%
7-8	1,12	1,10	1,8%	9-8	1,08	1,09	0,9%
7-9	1,10	1,09	0,9%	9-9	1,09	1,11	1,8%
7-10	1,08	1,09	0,9%	9-10	1,14	1,15	0,9%
8-1	1,00	0,98	2,0%	10-1	1,08	1,08	0,0%
8-2	1,01	1,00	1,0%	10-2	1,14	1,14	0,0%
8-3	1,08	1,07	0,9%	10-3	1,02	1,02	0,0%
8-4	0,94	0,94	0,0%	10-4	1,17	1,16	0,9%
8-5	1,11	1,12	0,9%	10-5	1,18	1,18	0,0%
8-6	1,01	1,00	1,0%	10-6	1,13	1,13	0,0%
8-7	1,15	1,16	0,9%	10-7	1,16	1,16	0,0%
8-8	1,09	1,09	0,0%	10-8	1,00	1,01	1,0%
8-9	1,07	1,08	0,9%	10-9	1,00	1,01	1,0%
8-10	1,12	1,11	0,9%	10-10	0,82	0,83	1,2%

Table 7: Two measurements of the intensity of the different light emitting diodes at 16 mA, and the percentage of difference between them.

4.3.1. Radiant power over time

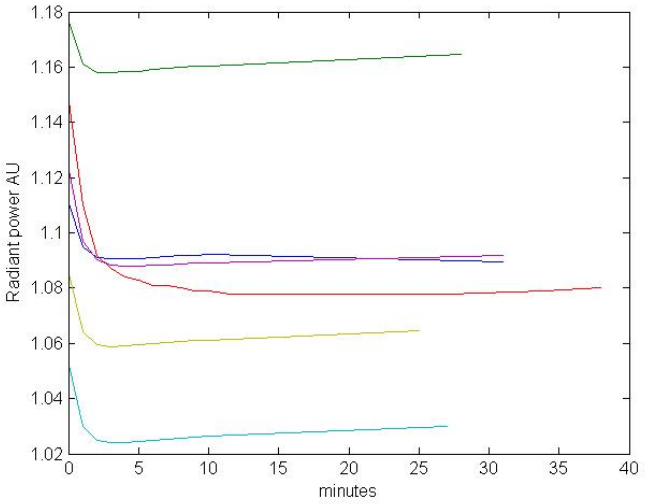

Figure 44: The intensity of six diodes measured over time.

4.3.2. Linearity of radiant power

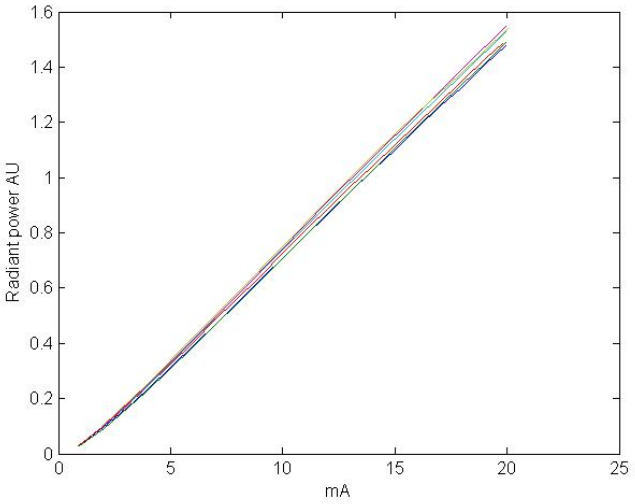

Figure 45: The measured intensity of six diodes against the applied current.

4.4. Noise

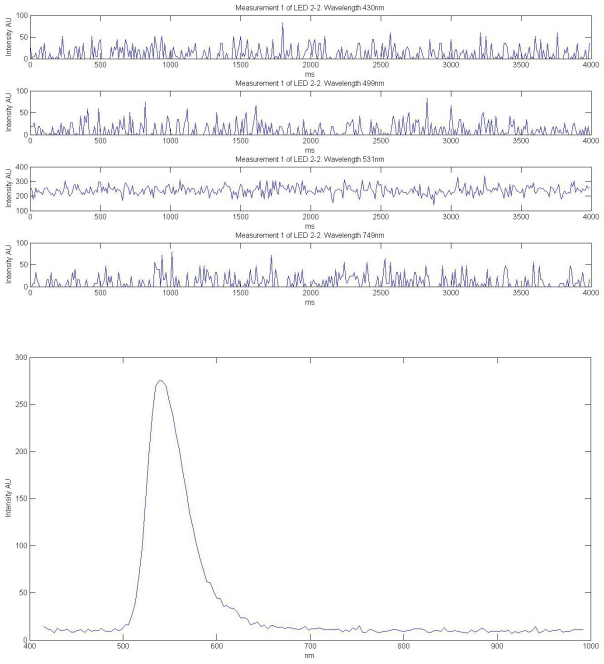

Figure 46: 400 lines from the measurement of LED 2-2, with a frame period of 10 ms, the lower image is a representation of the spectrum measured over the same 400 lines.

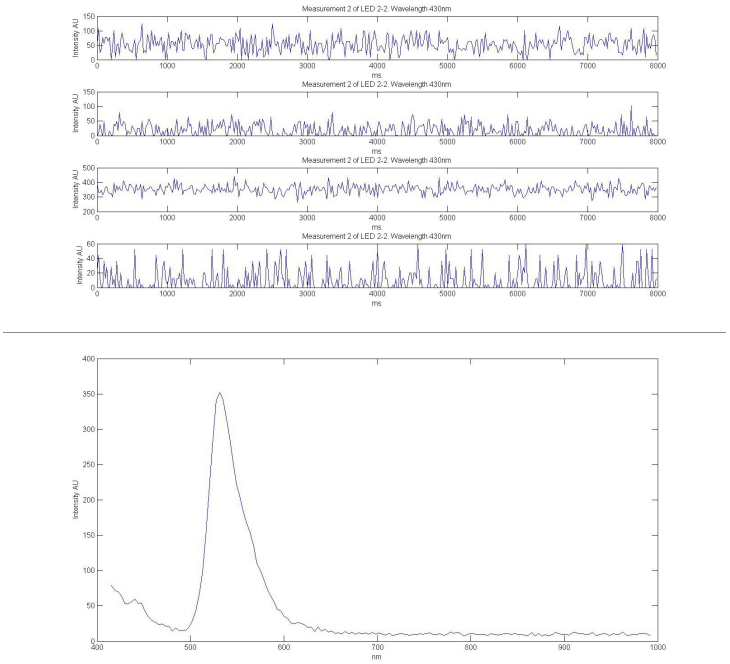

Figure 47: 400 lines from the measurement of LED 2-2, with a frame period of 20 ms, the lower image is a representation of the spectrum measured over the same 400 lines.

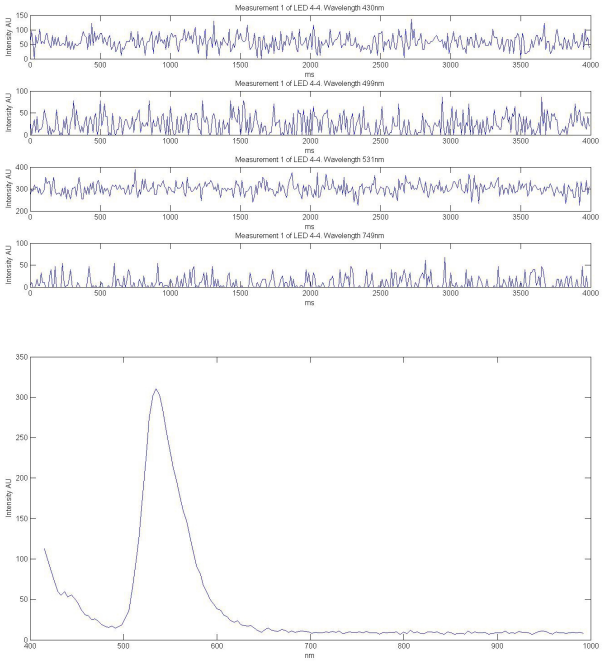

Figure 48: 400 lines from the measurement of LED 4-4, with a frame period of 10 ms, the lower image is a representation of the spectrum measured over the same 400 lines.

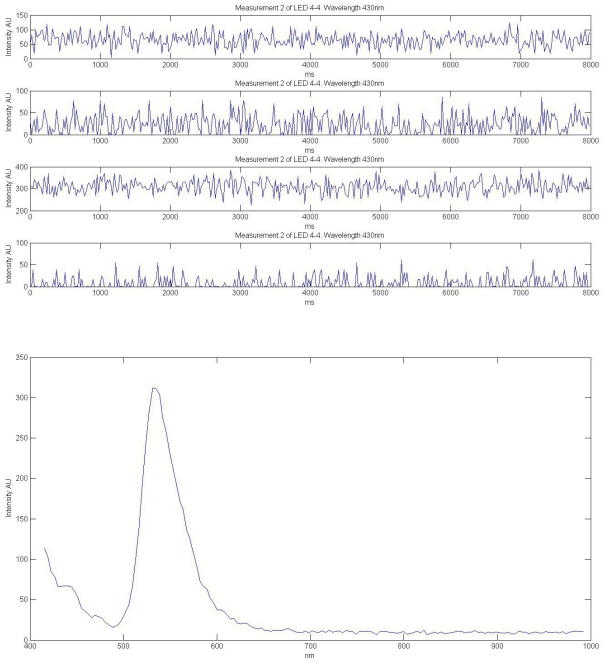

Figure 49: 400 lines from the measurement of LED 4-4, with a frame period of 20 ms, the lower image is a representation of the spectrum measured over the same 400 lines.

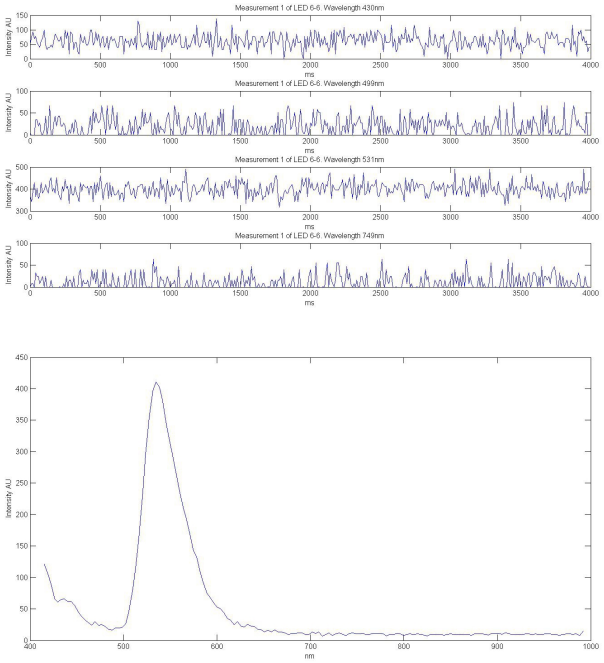

Figure 50: 400 lines from the measurement of LED 6-6, with a frame period of 10 ms, the lower image is a representation of the spectrum measured over the same 400 lines.

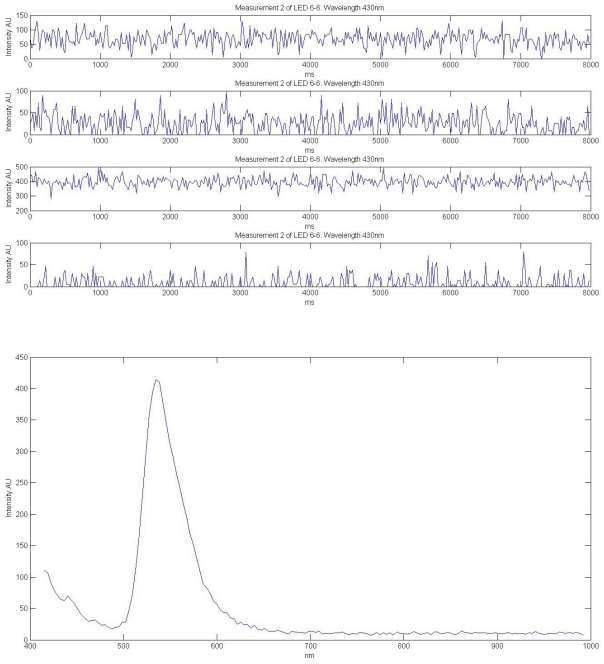

Figure 51: 400 lines from the measurement of LED 6-6, with a frame period of 20 ms, the lower image is a representation of the spectrum measured over the same 400 lines.

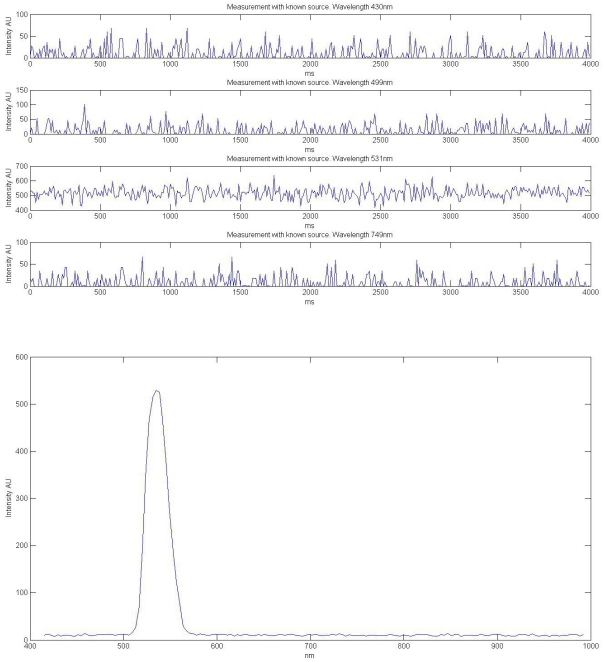

Figure 52: 400 lines from the measurement of the reference light source, with a frame period of 10 ms, the lower image is a representation of the spectrum measured over the same 400 lines.

4.5. Light source

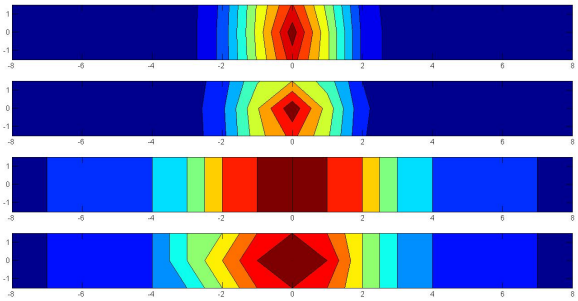

Figure 53: The field measurements of the light source powered by a single light emitting diode. The top figure shows the field without a lens or a diffuser, the second with a lens, the third with a diffuser and the fourth with both a lens and a diffuser.

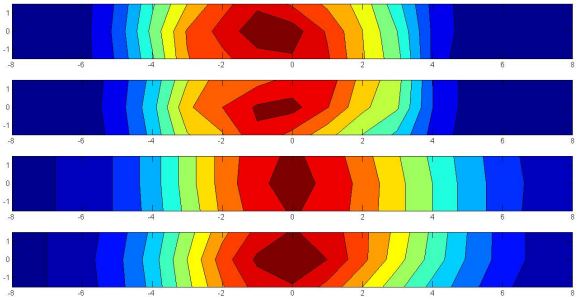

Figure 54: The field measurements of the light source powered by ten light emitting diodes with a distance of 0,75 cm between the center of each diode. The top figure shows the field without a lens or a diffuser, the second with a lens, the third with a diffuser and the fourth with both a lens and a diffuser.

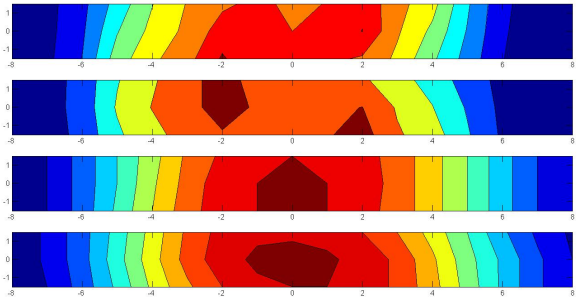

Figure 55: The field measurements of the light source powered by ten light emitting diodes with a distance of 1,00 cm between the center of each diode. The top figure shows the field without a lens or a diffuser, the second with a lens, the third with a diffuser and the fourth with both a lens and a diffuser.

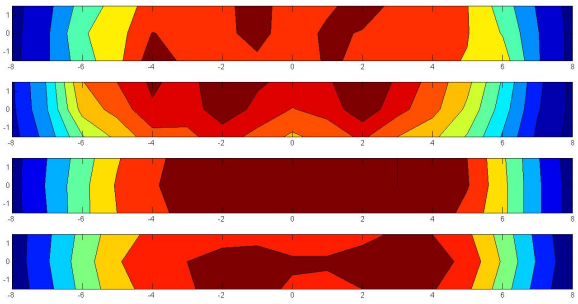

Figure 56: The field measurements of the light source powered by ten light emitting diodes with a distance of 1,25 cm between the center of each diode. The top figure shows the field without a lens or a diffuser, the second with a lens, the third with a diffuser and the fourth with both a lens and a diffuser.

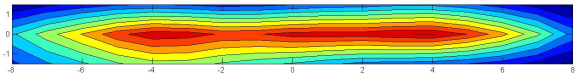

Figure 57: A field measurement of a reference light source.

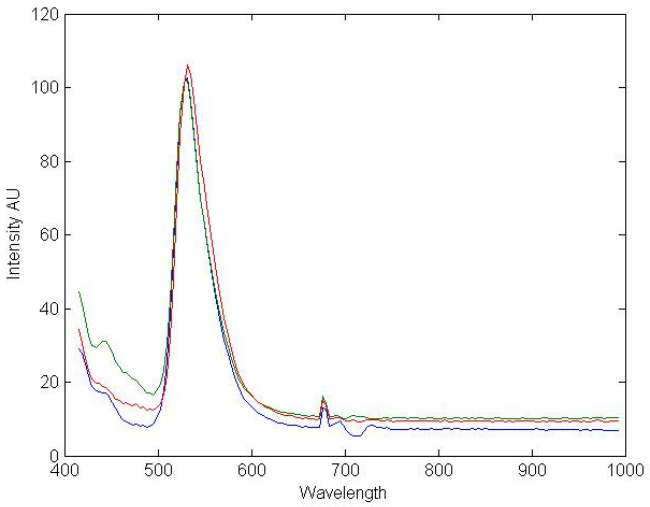

Figure 58: Three spectral measurements of different drops of fluorescein sodium on paper.

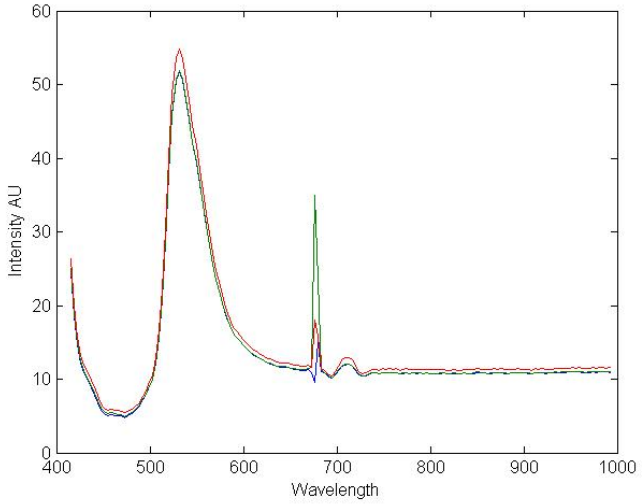

Figure 59: Three spectral measurements of fluorescein sodium inside a test tube.

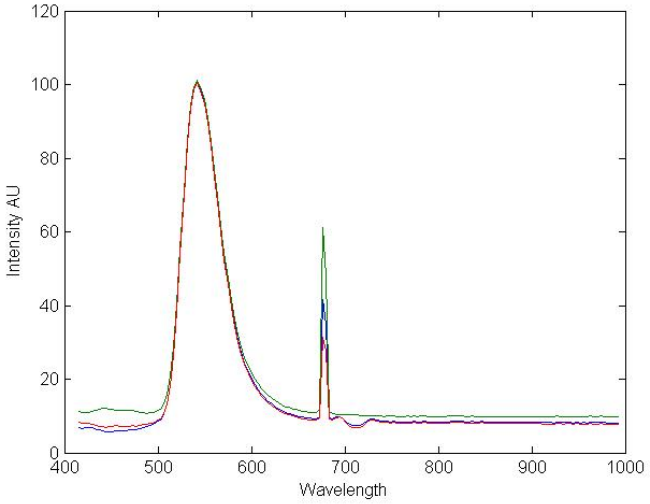

Figure 60: Three spectral measurements of fluorescein sodium in a weighing ship.

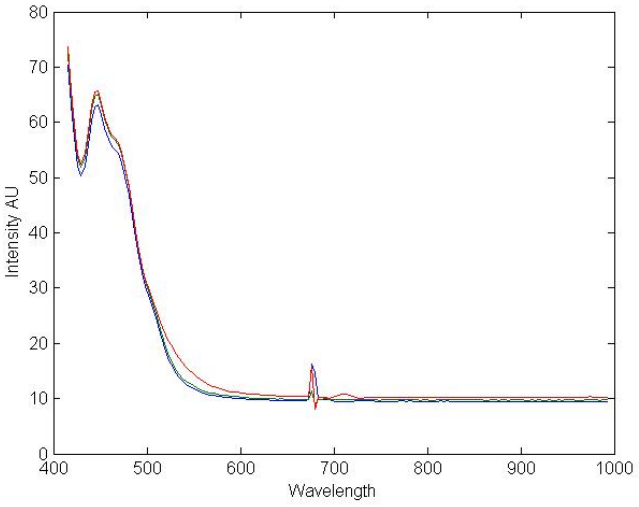

Figure 61: Three spectral measurements of paper.

5. Discussion

The figure 28 shows that there is a difference in the emitted wavelength from the diodes, but there are a few repeating wavelength peaks. In the figures 29, 30, 31, 32, 33, 34 and 35 the spectra were sorted into groups depending on their wavelength peak. The difference between the radiant power in the spectra can be ignored at this point, as there never were any measurement of the amount of damping the signal was exposed to. One of the big advantages with a LED light source is its narrow spectrum, arbitrarily chosen diodes could result in a broadening of the light source spectrum. Arbitrarily chosen diodes could also result in spectral variations in the field of light. The diodes should be chosen from the same group, or at least from groups with similar spectra.

The measurements of changes in the spectra due to heat were not as accurate as it should be, better equipment than a hairdryer would be needed. But even though they are quite rough the results shown in the figure 36 is clear, the wavelength changes rapidly due to heat. A common effect seems to be an increase of 1 nm from $25°$C to $30°$C, and another 1 nm before the temperature reaches $40°$C. The temperature needs to be monitored, and maybe controlled.

The figures 37, 38, 39 and 40 shows little to no difference in the spectrum of each diode due to time, there was a clear change in the radiant power, but this was explored in greater detail in other measurements.

The viewing angle of 14 LEDs was measured, the results can be seen in the figures 41, 42 and 43. The data sheet in appendix A gives the LEDs a viewing angle of $15°$, the results from the measurements do confirm this. Inaccuracy in these measurements seem to be noticeable and any real conclusions can not be drawn. But it can be used as a confirmation of already given information, as the measurements follow, to a degree, the information given in the data sheet.

The tables 6 and 7 shows the radiant power of the light emitting diodes in arbitrary units. The two main purposes of these measurements were to show that the method was stable and to measure the radiant power of the diodes against each other. The first ten diodes were a part of another experiment shortly before the first measurement, therefore they were omitted from the first measurement. Most of the diodes were measured with quite similar values, the difference was 1% or less. Human error plays a big part in the differences seen between the measurements, as the experiment requires the diodes to be placed in the exact same position in every measurement. Therefore the differences were not unexpected, but the experiment was accurate enough for the purpose of this work. Do the groups found in the spectrum measurements, see the figures 29, 30, 31, 32, 33, 34 and 35, have any impact on the radiant power of the diodes? There seems to be little or no correlation between the amount of radiant power and the wavelength of the diodes' spectral peak. But the radiant power of the diodes are quite similar, at least in most of the diodes, and the difference could easily be compensated for with individual current values.

Figure 44 shows that the radiant power of the LEDs drops a noticeable amount in the first few minutes. The change in the radiant power did not stop after the initial minutes, but the decrease slowed down and eventually the radiant power started to increase. But the changes after the first few minutes were insignificant compared to the value of the radiant power. The largest drop in the measured diodes were $6 - 7\%$, the others had a

$\approx 2\%$ drop. The initial drop is easily avoidable by waiting a few minutes before using the light source, the diodes were not prone to this drop if they had been recently used.

The linearity of the radiant power response of a few diodes can be seen in figure 45. Even though there were differences in the responses, they were small compared to the overall radiant power. The responses follow a clear linear line.

The figures 46, 47, 48, 49, 50 and 51 show fluorescence induced by three different light emitting diodes at two different frame periods. The noise displayed in these figures are quite similar and seems random, with an average amplitude of 50. With the fact that this noise is shared by the reflectance image of the reference light source, 52, it is safe to assume that this noise can be attributed to the hyperspectral camera. Even if it was assumed that the noise from the constant current regulators was not reduced during the fluorescence process, it would still be small compared to the noise from the camera and it can be ignored.

Figure 53 shows the field of a single point light source. The field improved with the diffuser, but it was far from good enough to be used. The uniform field was only two centimeters, the reference field, 57, is uniform in ten centimeters. The field from the point source was also very weak. The field shown in figure 54 was not weak, but it had a field that was similar to the point source. The reason for this can be seen by comparing the field to the figure 24. The diodes have a large impact on the field of its nearest neighbours, and an influence of a lesser degree farther away. The center was therefor influenced by almost all the diodes and produced a field similar to a point source. This large impact on the neighbouring fields made the field of the whole light source hard to control.

When measuring the field of the two light sources represented in the figures 55 and 56, the current was kept at a constant level after the initial 18 mA were set on each diode. The neighbour effects did not work against the uniformity of the field. Figure 55 shows a field that still is not uniform in a large enough area, the field should be uniform in approximately ten centimeters, something the light source shown in figure 56 manages. The field in figure 56 originally shows signs that it had several point sources and not a uniform source, but the diffuser removed most of these effects.

The spikes around 700 nm in the spectra shown in the figures 58, 59, 60 and 61 are due to a laser used for focusing, they can be ignored. The three spectra in each of these figures should in theory be identical, as long as the line field of the light source was uniform. There were many potential sources of error in these measurements, for example bulks in the paper and different amounts of fluorescein sodium. Fluorescein sodium were put in different containers to counteract these sources of error, but other problems arose. In closed containers, as the test tube 59, the light had to traverse an extra layer before interacting with the fluorescent material and again before it could be recorded by the camera. But the main problem was the size of the containers, they could not cover the whole field. The measurements of the fluorescent liquid in the weighing ship eliminated most of the serious sources of error, but it also covered less than half of the field. The spectra in figure 60 are almost identical, although this is good, measurements covering the whole field were needed. The measurements of fluorescein drops on paper and blank paper, 58 and 61, were subjected to more sources of error, but the spectra in the figures were taken from both ends and the middle of the field.

By comparing the field of the reference light source, 57, and the field of the light

source used, 56, in addition to the results from the fluorescence measurements, 58, 59, 60 and 61, the uniformity of the field can be regarded as good enough. But something that is clear from the comparison of the figures 57 and 56 is that the width of the field is too large. This results in unnecessary bleaching of the fluorescent material and needs to be resolved. The lens used in this work was a lens designed for the existing light source of the hyperspectral camera, either a new lens should be acquired or the numerical aperture of the light source should be reduced.

6. Conclusion

A light source based on a line of light emitting diodes pose a few problems, but it was proven to be useable. Further work is needed and the most important issues that need to be resolved is the width of the light field, the size of the current source and the loss of uniformity near the edges.

The uniformity of the field being was a large problem, as the light source is basically a row of point sources. This problem was met by keeping the distance between each diode at a level where the fields interacted with each other and made a more constant field, together with a diffuser a uniform field was accomplished. But the uniformity of the field dropped near the edges, because the neigbour effects were different on the edge diodes compared to the others. This can be improved by introducing more diodes, which are placed beyond the edges of the numerical aperture.

The current source used for the final light source used in this work was ten constant current regulators, see appendix B. A future current source should be able to change the level of current both on each diode individually and simultaneously on all the diodes. The individual setting to prevent the diodes from emitting different amounts of light and the simultaneous setting to change the radiant power of the light source as a whole. A constant current regulator with several channels might accomplish this, as well as reducing it to a manageable size.

A future light source should decrease the numerical aperture from its current state, to reduce the width of the light field. Some of this reduction of width could be accomplished by introducing a new lens, which would also increase the intensity of the field.

References

[1] M.C. Teich B.E.A. Saleh. *Fundamentals of photonics*. Wiley, 2007.

[2] C. F. Bohren. Multiple scattering of light and some of its observable consequences. *American Journal of Physics*, 55(6):524–533, 1987.

[3] C.I. Chang. *Hyperspectral data exploitation: theory and applications*. Wiley-Interscience, 2007.

[4] C. Gordon. A generalization of the maximum noise fraction transform. *IEEE Transactions on geoscience and remote sensing*, 38:608–610, 2000.

[5] A.A. Green, M. Berman, P. Switzer, and M.D. Craig. A transformation for ordering multispectral data in terms of image quality with implications for noise removal. *IEEE Transactions on geoscience and remote sensing*, 26:65–74, 1988.

[6] A. Ishimaru. Diffusion of light in turbid material. *Applied Optics*, 28:2210–2215, June 1989.

[7] J. R. Lakowics. *Principles of Fluorescence Spectroscopy*. Springer, 2006.

[8] E.L.P. Larsen. *Biomedical applications of diffuse reflectance spectroscopy and hyperspectral imaging*. PhD thesis, Norges teknisk-naturvitenskaplige universitet, 2010.

[9] B. Lasorne, G.A. Worth, and M.A. Robb. Excited-state dynamics. *Wiley Interdisciplinary Reviews: Computational Molecular Science*, 1(3):460–475, 2011.

[10] L.L. Randeberg, E.L.P. Larsen, A. Aksnes, O.A. Haugen, and L.O. Svaasand. Hyperspectral characterization of atherosclerotic plaques. *Proceedings of SPIE*, 7368:736808, 2009.

[11] L.L. Randeberg, E.L.P. Larsen, and L.O. Svaasand. Hyperspectral imaging of blood perfusion and chromophore distribution in skin. *Proceedings of SPIE*, 7161:71610C, 2009.

[12] L.L. Randeberg, A.M. Winnem, E.L.P. Larsen, M.B. Lilledahl, R. Haaverstad, O.A. Haugen, and L.O. Svaasand. In vivo hyperspectral imaging of traumatic skin injuries in a porcine model. *Proceedings of SPIE*, 6424:642408, 2007.

[13] R. W. Redmond. *Handbook of Biomedical Fluorescence*. Marcel Dekker, 2003.

[14] L.S. Saidi, S.L. Jacques, and F.K. Tittel. Mie and rayleigh modeling of visible-light scattering in neonatal skin. *Applied Optics*, 34:7410–7418, 1995.

[15] T. Spott. *Characterization of layered tissue structures with diffusely propagating photon density waves*. PhD thesis, Norges teknisk-naturvitenskaplige universitet, 1999.

[16] K. Streubel. *Handbook of Optoelectronics*. Taylor & Francis Group, 2006.

[17] D.F. Swinehart. The beer-lambert law. *Journal of chemical education*, 39:333–335, 1962.

[18] L.V. Wang and H. Wu. *Biomedical optics*. Wiley, 2007.

A. Data sheet of light emitting diodes

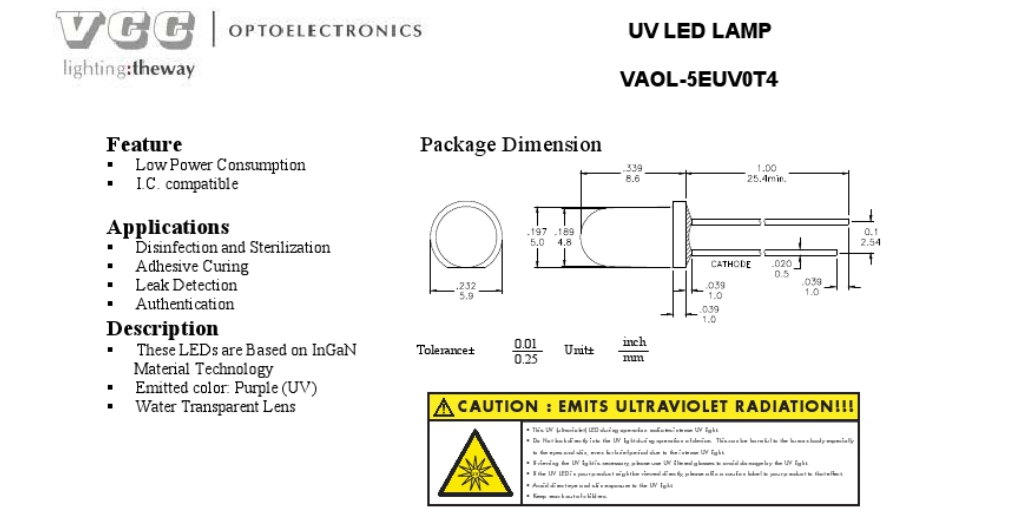

VCC | OPTOELECTRONICS
lighting:theway

UV LED LAMP

VAOL-5EUV0T4

Feature
- Low Power Consumption
- I.C. compatible

Applications
- Disinfection and Sterilization
- Adhesive Curing
- Leak Detection
- Authentication

Description
- These LEDs are Based on InGaN Material Technology
- Emitted color: Purple (UV)
- Water Transparent Lens

Package Dimension

Tolerance± 0.01/0.25 Unit± inch/mm

CAUTION : EMITS ULTRAVIOLET RADIATION!!!

Absolute Maximum Ratings at Ta=25°C

Symbol	Parameter	Max.	Unit
PD	Power Dissipation	120	mW
VR	Reverse Voltage	5	V
IAF	Average Forward Current	30	mA
IPF	Peak Forward CurrentDuty0.1 1kHz	100	mA
—	Derating Linear Form 25°C	0.4	mA/°C
Topr	Operating Temperature Range	–20 to 80	°C
Tstg	Storage Temperature Range	–20 to 100	°C
Lead Soldering Temperature [1.6mm 0.063inch From Body] 260°C For 5 Seconds.			

Electrical / Optical Characteristics and Curves at Ta=25°C

Symbol	Parameter	Test Condition	Min.	Typ.	Max.	Unit
VF	Forward Voltage	IF 20 mA	2.8	3.0	3.6	V
IR	Reverse Current	VR 5 V			50	μ A
$\Delta\ \theta$	Half Intensity Angle	IF 20 mA	10	15	20	Deg.
IV	Luminous Intensity	IF 20 mA	--	200	--	mcd.
λ p	Peak Wavelength	IF 20 mA	400	405	--	nm

www.vcclite.com
990 bosstick blvd, ste 101
san marcos, ca 92069
phone 760.560.1300
fax 760.560.1301

RoHS
ISO 9001 Registered

Figure 62: Page 1 of the data sheet.

VCC | OPTOELECTRONICS
lighting:theway

Electrical Characteristics at Ta=25℃

Symbol	Iv		VF		λp	
Parameter	Luminous Intensity		Forward Voltage		Peak Wavelength	
Condition	IF=20mA		IF=20mA		IF=20mA	
Unit	mcd		V		nm	
Binning	Grade	Range	Grade	Range	Grade	Range
	BIN10	125~175	P0	2.8~3.0	U6	400~405
	BIN11	175~245	P1	3.0~3.2	U7	405~410
			P2	3.2~3.4		
			P3	3.4~3.6		

Intensity: Tolerance of minimum and maximum = ± 15%
Vf. Tolerance of minimum and maximum = ± 0.05v
NOTE:
1. Static electricity and surge damages the LED. It is recommend to use a anti-static wrist band or anti-electrostatic glove when handing the LEDs. All devices, equipment and machinery must be properly grounded.

Radiation Diagram

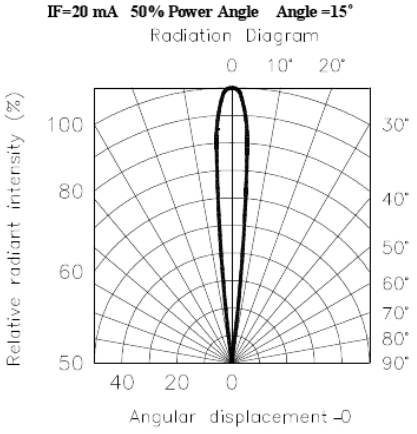

Figure 63: Page 2 of the data sheet.

VCC | OPTOELECTRONICS
lighting:theway

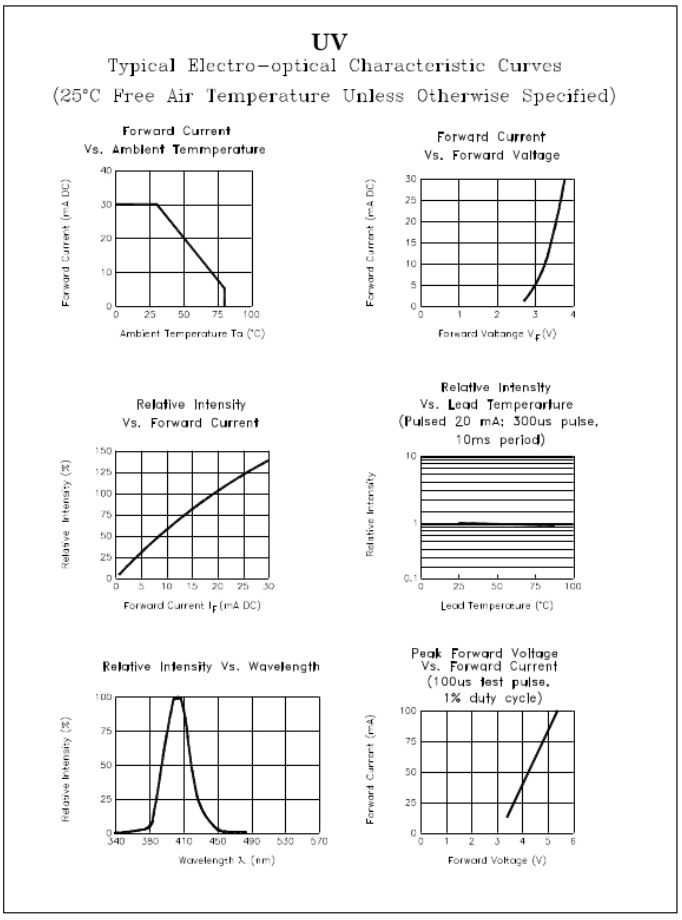

Figure 64: Page 3 of the data sheet.

B. Current regulator

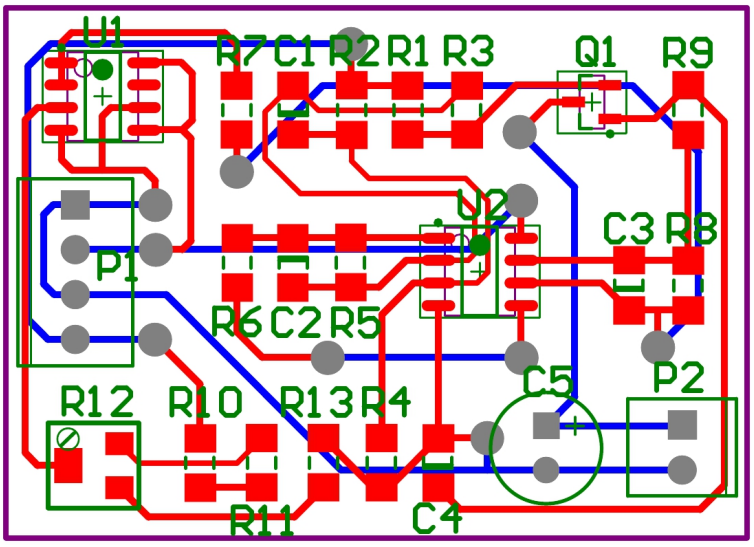

Figure 65: PCB prints of the constant current regulators.

Bill of Materials — Constant Current Regulator

Source Data From:	Constant-Current-Regulator.PrjPcb
Project:	Constant-Current-Regulator.PrjPcb
Variant:	None
Creation Date:	11.04.2012 13:35:46
Print Date:	41010 41010,56656

#Column Nam	#Column Name E	#Column Name E	Designator	Description	Quantity
			C1, C2, C3, C4	Ceramic Chip Capacitor - Standard	4
			C5	Polarized Capacitor (Radial)	1
			P1	Header 4 pin with 2.54mm pitch	1
			P2	Header 2 pin	1
			Q1	P-channel Enhancement Mode MOSFET	1
			R1, R2, R3, R4, R5, R6, R7, R8, R9, R10, R11, R13	Resistor	12
			R12	Potentiometer	1
			U1	Dual Low-Power Operational Amplifier	1
			U2	Dual Operational Amplifier	1
					23

Approved	Notes	

Figure 66: The bill of materials for the PCB prints.

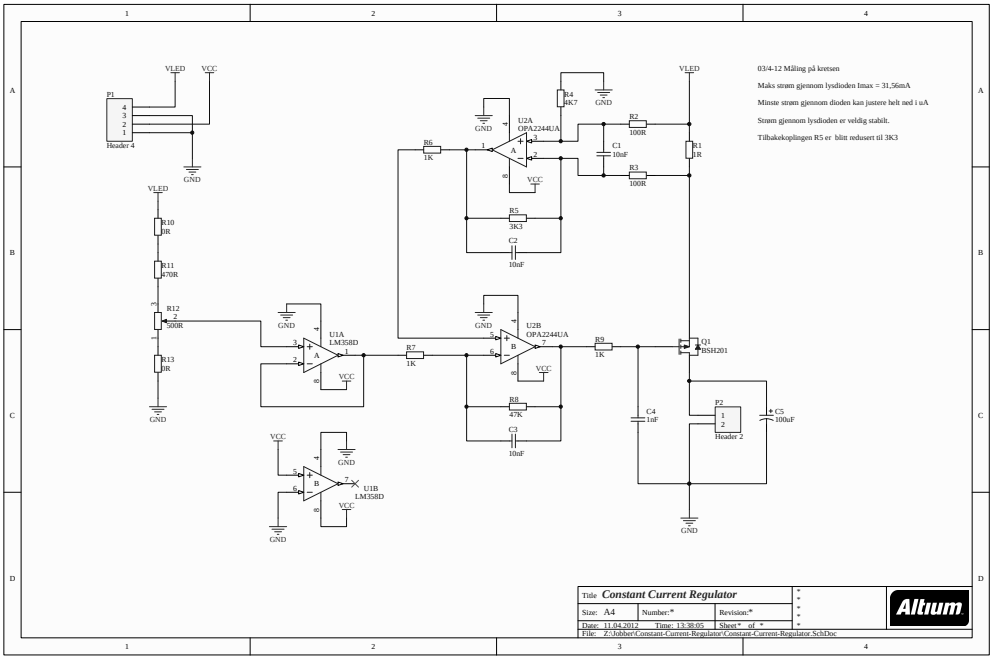

Figure 67: The schematic prints of the constant current regulators.

Description	Manufacturer	Manufacturer Part Number	Supplier	Supplier Part Number	Technology	Quantity
Polarized Capacitor (Radial)	MULTICOM	MCRH25V107M6.3X11	Farnell	9451838	THT	3
Header 2 pin with 2.54mm pitch	PHOENIX CONTACT	1725656	Farnell	3041359	THT	5
Header 4 pin with 2.54mm pitch	TE CONNECTIVITY / BUCHANAN	282834-4	Farnell	1767502	THT	5
P-channel Enhancement Mode MOSFET	NXP	BSH201,215	Farnell	1758073	SMD	10
Resistor 1ohm	PANASONIC	ERJ14BQF1R0U	Farnell	1717932	SMD	10
LED 5mm Green	LED TECHNOLOGY	L02R5000Q1	Farnell	1208851	THT	5
Potentiometer 500ohm	BOURNS	3214W-1-501E	Farnell	1463557	SMD	5
Dual Low-Power Operational Amplifier	TEXAS INSTRUMENTS	LM358D	Farnell	1648685	SMD	5
Dual Low-Noise Operation Amplifier	ON SEMICONDUCTOR	MC33078DG	Farnell	9665323	SMD	5
Dual Operational Amplifier	TEXAS INSTRUMENTS	OPA2244UA	Farnell	1212438	SMD	5

Figure 68: Table of the components used in the regulators.

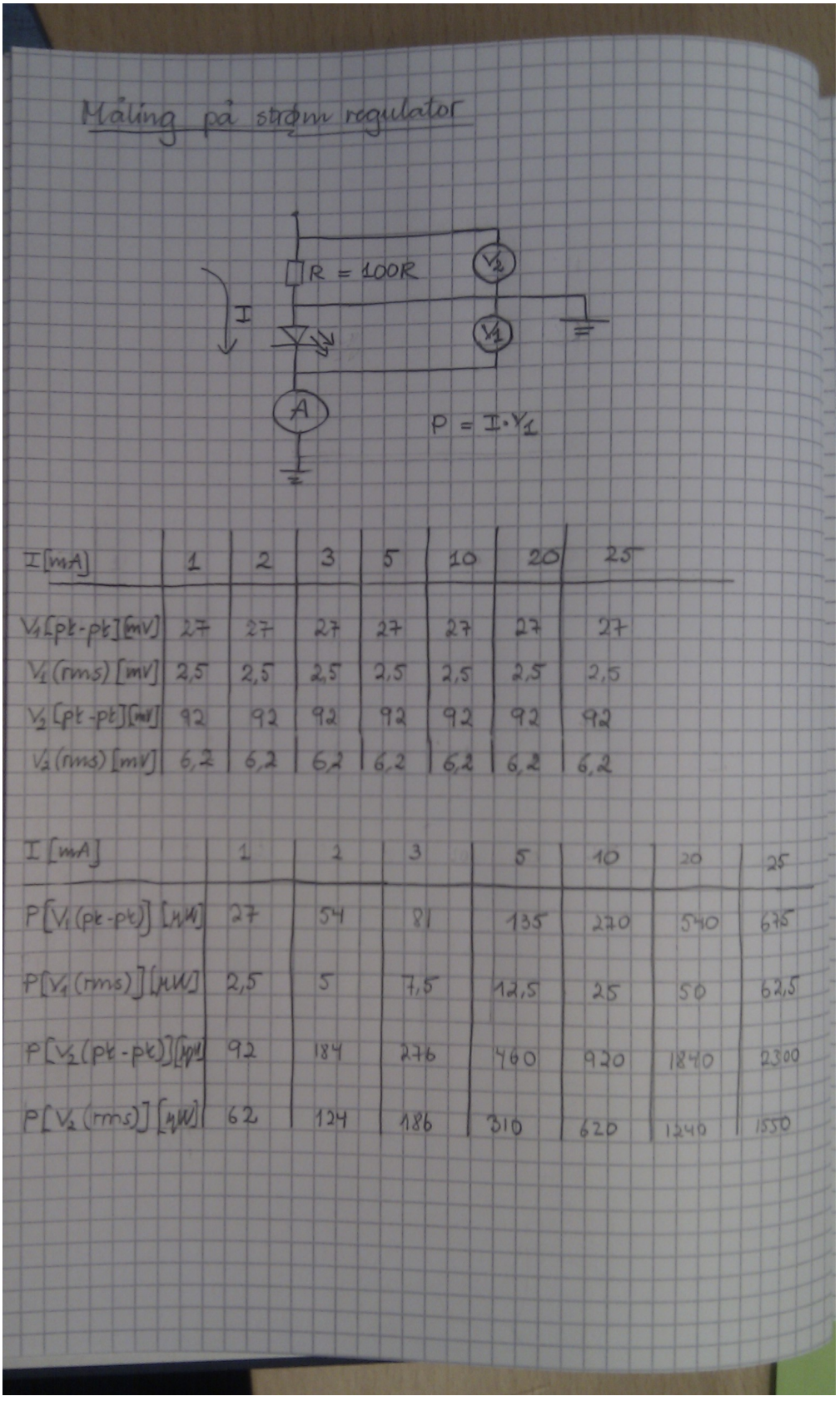

I [mA]	1	2	3	5	10	20	25
V_1 [pk-pk] [mV]	27	27	27	27	27	27	27
V_1 (rms) [mV]	2,5	2,5	2,5	2,5	2,5	2,5	2,5
V_2 [pk-pk] [mV]	92	92	92	92	92	92	92
V_2 (rms) [mV]	6,2	6,2	6,2	6,2	6,2	6,2	6,2

I [mA]	1	2	3	5	10	20	25
P [V_1 (pk-pk)] [µW]	27	54	81	135	270	540	675
P [V_1 (rms)] [µW]	2,5	5	7,5	12,5	25	50	62,5
P [V_2 (pk-pk)] [µW]	92	184	276	460	920	1840	2300
P [V_2 (rms)] [µW]	62	124	186	310	620	1240	1550

Figure 69: Results from the tests on the first constant current regulator.